A molecular dynamics investigation of the dissolution of molecular solids

by

Abhinav Anand

B.Tech., I.I.T. Guwahati, 2015

A THESIS SUBMITTED IN PARTIAL FULFILLMENT OF
THE REQUIREMENTS FOR THE DEGREE OF

MASTER OF SCIENCE

in

The Faculty of Graduate and Postdoctoral Studies

(Chemistry)

THE UNIVERSITY OF BRITISH COLUMBIA

(Vancouver)

September 2017

Abstract

The dissolution of molecular solids is an important process, which has been studied for over a century. However, a lot of work is still needed for a detailed understanding of the molecular mechanism of dissolution, because of the complex nature of many molecular solids, and the large time scales required for simulation studies. In this thesis we study the dissolution of molecular solids, to examine if classical models (which assume that the rate is proportional to an active surface area) can be used to describe the dissolution profile of these solids.

Urea and aspirin molecules are used as models, to study the dissolution process in water under sink conditions, because of their contrasting solubility in water. The dissolution rate in different water models was examined and it was found that they differ considerably. However, the overall mechanism for the dissolution process remains the same. Dissolution was found to be an activated process with the detachment of molecules from the crystal being the rate limiting step. Crystals with different shapes (cubic and cylindrical) were used to study the effect of shape on the dissolution process.

The dissolution process for urea was found to occur in three steps, an initial rapid stage, where the molecules at the edges and corners go into the solution, a long intermediate stage with a nearly constant dissolution rate, and a final stage where the crystals lose their crystalline structure and dissolve completely. The fixed rate law stage was found to be described by a simple rate law derived from classical models.

It was found that there is an additional step in the dissolution process for aspirin, occurring between the initial rapid stage and the fixed rate law stage, during which the crystal attains a solution annealed shape. The fixed rate law stage was again found to be described by a simple rate law.

The results obtained are in agreement with an earlier dissolution study of NaCl crystals, thus it appears that the classical rate laws can be used to describe the dissolution of a variety of complex molecular and ionic crystals.

Lay Summary

Dissolution of molecular solids is an important process in many physical systems and situations. However, a lot of work is still needed for a detailed understanding of the molecular mechanism of dissolution, because of the complex nature of many molecular solids, and the large time scales required for simulation studies. My study was focused on uncovering the molecular mechanism of dissolution, and employed molecular dynamics simulation to investigate the complete dissolution of molecular solids. Urea and aspirin molecules are used as models. I found that these crystals dissolve in a simple three step process, and under sink conditions, detachment of the molecules from crystal is the rate limiting step. I also found that the dissolution profile can be described by simple rate laws to a very good extent. Thus, it appears that these laws can be used to describe the dissolution of a variety of complex molecular and ionic crystals.

Preface

The research presented in the thesis are based on work done by me in Dr. G. N. Patey's group. The chapters 3 and 4 are part of articles that will be published by A. Anand and G. N. Patey.

The projects were designed by me with Dr. G. N. Patey, and are extensions of a previous project, done by G. Lanaro, doctoral student in Dr. G. N. Patey's group, which investigated the dissolution of ionic nanocrystals of NaCl.

In all the projects, I performed the simulations, developed programs for data analysis, and formulated the hypothesis with suggestions, and guidance from Dr. G. N. Patey. The manuscripts for the articles have been written by me with revisions and additions by Dr. G. N. Patey.

Table of Contents

List of Tables

List of Figures

List of Symbols and Abbreviations

k_B	Boltzmann Constant
d	Bond Length
θ	Bond Angle
ϕ	Dihedral Angle
q	Point Charge
$\mathcal{K}$	Kinetic Energy
$\mathcal{V}$	Potential Energy
f	Force
D	Diffusion Coefficient
E_a	Activation Energy
u_C	Coulombic Potential
u_{LJ}	Lennard-Jones Potential
σ	Lennard-Jones Length Parameter
ϵ	Lennard-Jones Energy Parameter
API	Active Pharmaceutical Ingredients
GROMACS	GROningen Machine for Chemical Simulations
LINCS	Linear Constraint Solver
LJ	Lennard-Jones
MD	Molecular Dynamics
PME	Particle Mesh Ewald
PBC	Periodic Boundary Conditions

SPC	Single Point Charge Model
SPC/E	Extended Single Point Charge Model
TIP3P	Three-site Transferable Intermolecular Potential Model
TIP4P/2005	Four-site Transferable Intermolecular Potential Model of 2005
GAFF	Generalized AMBER Force Field
AMBER	Assisted Model Building with Energy Refinement
CHARMM	Chemistry at HARvard Macromolecular Mechanics
MMFF	Merlock Molecular Force Field

Acknowledgements

I would like to thank my supervisor Dr. Gren Patey, for all his help, encouragement and enthusiastic discussions throughout these last two years. I would also like to thank the lab members, and all the friends I have met here, for all the fun during work and life in general.

And finally, I would like to thank my family for all the support.

Chapter 1

Introduction

1.1 Foundation of dissolution research

The study of dissolution processes has been developing since the late 1800's, and the first dissolution study was reported in the literature by Arthur A. Noyes and Willis R. Whitney in 1897 in an article[1] entitled "The rate of solution of solid substances in their own solutions". This laid the foundation for dissolution research for the next century, where different dissolution models based on various assumptions were suggested as physical explanations for the dissolution process.

Noyes and Whitney suggested that the dissolution rate can be predicted with high accuracy by considering the dissolution process as a process of diffusion, where the molecules diffuse into the solution from a thin diffusion layer formed around the solid. The mathematical expression of the law that they proposed is the famous Noyes-Whitney equation

$$\frac{dc}{dt} = K(c_s - c_t) \ , \tag{1.1}$$

where $\frac{dc}{dt}$ is the dissolution rate, K is the rate constant, c_s is the solubility of the substance, and c_t is the concentration of the dissolved substance at time t.

They performed an experiment measuring the concentration of benzoic acid and lead chloride in water and calculated the K value at various time points. They found the values calculated to be very similar, confirming their hypothesis of a "diffusion controlled dissolution".

In 1900 Erich Brunner and Stanislaus von Tolloczko published an article[2] which considered

the dependence of dissolution on the exposed surface area. They proposed an expression which was derived from Equation (1.1) by letting, $K = K_1 S$

$$\frac{dc}{dt} = K_1 S(c_s - c_t) \ , \tag{1.2}$$

where S is the exposed surface area of the solid. The models presented above did not consider any time dependent changes in the surface area of the solid during dissolution. Hixson and Crowell[3] addressed the fact that the surface of the dissolving solid changes with time and obtained an expression for dissolution rate,

$$\frac{dM}{dt} = -K^{'} S_t(c_s - c_t) \ , \tag{1.3}$$

where dM is the amount of the substance which dissolved in the time interval dt, $K^{'}$ is a constant, S_t is the available surface area, c_s is the solubility in the bulk fluid, and c_t is the concentration of the dissolved substance at time t.

For cases when the change in concentration of the dissolved substance in the bulk fluid is negligible (perfect sink conditions), "$c_s - c_t$" can be considered as a constant. Thus $k^{'}$ and "$c_s - c_t$" can be combined to a new constant $k^{''}$ such that,

$$\frac{dM}{dt} = -K^{''} S_t \ . \tag{1.4}$$

For a spherical particle with radius R_t at time t the surface area, S_t can be written as $S_t = 4\pi R_t^2$, the volume of the particle v_t as, $v_t = \frac{4}{3}\pi R_t^3$, and since "$mass \propto Volume$", one can express surface area as a function of mass in the following way: $S_t = constant \times M_t^{\frac{2}{3}}$. Thus the Equation (1.4) can be written as

$$\frac{dM}{dt} = -K^{'''} M_t^{\frac{2}{3}} \ , \tag{1.5}$$

with $K^{'''}$ being another constant and M_t being the remaining mass of the solid at time t. The

integrated form of the Equation (1.5) leads to the well known "Hixson-Crowell equation" or the "cube root law"

$$M_0^{\frac{1}{3}} - M_t^{\frac{1}{3}} = kt \ . \tag{1.6}$$

where M_0 and M_t denote the mass of the solid at time $t = 0$ and at time t, respectively, and k is a constant.

There are different explanations that have been proposed for the rate law expressions listed above. The first which assumes that diffusion through the surface layer is the limiting step of the dissolution process, was put forward by Brunner[4] and Nernst.[5] Another explanation came from Lanaro and Patey,[6] where they show that under sink conditions, the rate determining step is the detachment of the molecule from the crystal surface. Various other models have also been proposed as an alternative explanation to the dissolution process. The "interfacial barrier model" which considered interfacial transport rather than the diffusion through the layer as the limiting step, first proposed by Wilderman[7] and later considered by Zdanovskii,[8] has not been studied extensively. Another model proposed by Dankwerts[9] considered that constantly renewed packets of solvent reach the surface and absorb solute particles, delivering them to the solution. Combinations of these models have also been studied.

1.2 Recent trends in dissolution research

All the advances in in-vitro dissolution studies were achieved before 1950 by physical chemists laying the basic set of principles for the dissolution process. The second half of the 20th century saw a considerable amount of interest in dissolution studies again due to a couple of factors. First the relationship between dissolution rates and bioavailability[10,11] started to develop in the late 1950's and by the early 21st century in vitro dissolution testing emerged as a very important tool for the development and approval of safe and generic drug products.[12,13] This sparked considerable interest in the dissolution process of various crystalline solids.[14]

The second factor was the large increase in computational power, as a result of which molecular dynamics simulation studies of the dissolution process started to gain popularity in

the scientific community. These studies were conducted to uncover the steps of dissolution at the microscopic level, as the classical models discussed before presented very little information about the dissolution of nanocrystals. Piana and Gale[15] studied the dissolution and growth of the [001] surface of urea in contact with water. They found that the single surface dissolves quickly, forming a super saturated solution, which on cooling leads to rapid growth of the surface. Gao and Olsen[16] studied dissolution of the drug acetaminophen in water, and revealed the importance of corners and edges in the initial stages of the dissolution process.

Elts et. al.[17] studied the dissolution of aspirin using both Molecular dynamics simulation and Kinetic Monte Carlo techniques, and investigated the possibility of predicting dissolution rates for Active Pharmaceutical Ingredients (API) based on their molecular structures. However, because of the complex structures and low solubilities of these API's, the computational effort required for the study of the whole dissolution process of bigger molecules is not practical. Lanaro and Patey[6] investigated the dissolution of an ionic crystal, NaCl, in water, and analyzed the dissolution rate using some of the classical dissolution models discussed before. They found that these models provide a very good description of the intermediate stage of the dissolution profile. Using this technique they could predict the dissolution rate of NaCl in water by analyzing only a fraction of the full dissolution run.

Thus it is of interest to test if the same technique could be used for molecular solids, as this would help reduce the time scale required for the prediction of rates for APIs.

Chapter 2

Models and Methods

2.1 Overview

Simulation requires a model of the system that mimics the experimental properties of the sample for the conditions under investigation. Simulation also requires various methods to control the temperature, pressure, and the molecular geometry (chemical bonds and bond angles) of the system during evolution. In this chapter we discuss the models that are used for the dissolution studies of two different molecular solids (aspirin and urea) in water, and explain the various algorithm used during the simulation.

2.2 Water models

The different water models used in the dissolution studies are: Simple Point Charge (SPC) water model,[18] Extended Simple Point Charge (SPC/E) water model,[19] three point Transferable Intermolecular Potential (TIP3P)[20] water model, and the four point Transferable Intermolecular Potential (TIP4P/2005)[21] water model. The first three models (SPC, SPC/E, and TIP3P) have three interaction sites (one on each atom of the molecule), while the TIP4P/2005 water model has four interaction sites, with the fourth virtual site representing the lone pair placed at the bisector of the H−O−H angle. The molecular geometries of the different water model are displayed in Figure 2.1 and the geometric parameters, Lennard-Jonnes (LJ) parameters and the charges on the interaction sites are summarized in Table 2.1. The water models used are rigid and have slightly different Coulombic and LJ parameters. Different models are used to study the influence of the solvent model on the dissolution profile of molecular solids.

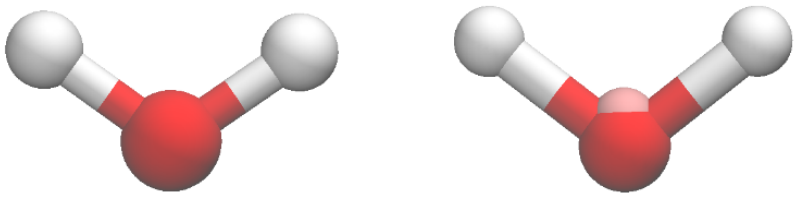

a) 3-site model b) 4-site model

Figure 2.1: Geometrical representation of the three and four site water models. The oxygen atoms are represented in red, hydrogen atoms in gray, and the virtual sites in pink, respectively.

	SPC	SPC/E	TIP3P	TIP4P/2005
$d_{\mathrm{O-H}}$ (nm)	0.1000	0.1000	0.0957	0.0957
$d_{\mathrm{O-M}}$ (nm)	n/a	n/a	n/a	0.0155
$\theta_{\mathrm{H-O-H}}$ (degree)	109.5	109.5	104.5	104.5
q_{O} (e)	-0.8200	-0.8476	-0.8340	0.0
q_{H} (e)	0.4100	0.4238	0.4170	0.5564
q_{M} (e)	n/a	n/a	n/a	-1.1128
σ_{O} (nm)	0.3016	0.3016	0.3151	0.3158
ϵ_{O} (kJ mol^{-1})	0.6500	0.6500	0.6364	0.7749

Table 2.1: Molecular geometry, LJ parameters, and partial charges on interaction sites for different water models. The oxygen atom, hydrogen atoms, and virtual sites are denoted by O, H, and M respectively. The distance between sites is denoted by d, the bond angle by θ, the charge by q, and σ and ϵ are the LJ parameters.

2.3 Urea model

There are a number of atomistic models for urea that have been put forward for simulation studies.[22] However, the model that best reproduces the observed molecular properties of urea crystal and solution is the improved generalized AMBER force field (GAFF)[23,24] model. The molecular geometry of urea is displayed in Figure 2.2 and the improved GAFF parameters are summarized in Table 2.2. The unit cell representation was taken from X-ray diffraction

studies, which have been conducted by many authors,[25–27] and is displayed in Figure 2.2.

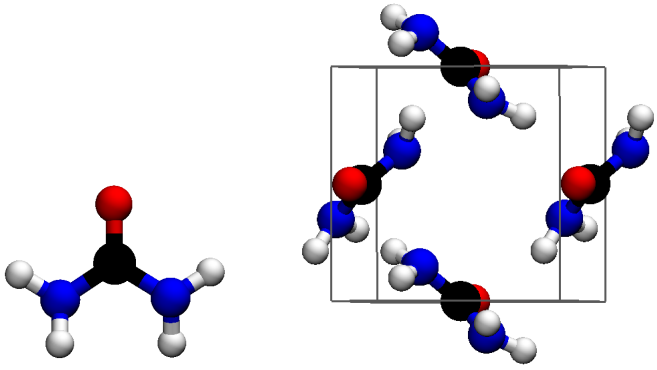

Figure 2.2: Geometrical representation of a single urea molecule and the unit cell of the urea crystal. The space group is $P\bar{4}2_1m$ and the unit cell dimensions are $a = b = 0.5565$ and $c = 4.684$ nm. The oxygen atom is represented in red, hydrogen atoms in gray, nitrogen atoms in blue, and the carbon atom in black.

$d_{\mathrm{C-O}}$ (nm)	$d_{\mathrm{C-N}}$ (nm)	$d_{\mathrm{N-H}}$ (nm)	
0.1250	0.1383	0.1010	
$K^d_{\mathrm{C-O}}$	$K^d_{\mathrm{C-N}}$	$K^d_{\mathrm{N-H}}$	
2744.70	1774.02	1815.86	
$\theta_{\mathrm{N-C-O}}$ (degree)	$\theta_{\mathrm{C-N-H}}$ (degree)	$\theta_{\mathrm{H-N-H}}$ (degree)	$\theta_{\mathrm{N-C-N}}$ (degree)
120.9	120.0	120.0	118.6
$K^\theta_{\mathrm{N-C-O}}$	$K^\theta_{\mathrm{C-N-H}}$	$K^\theta_{\mathrm{H-N-H}}$	$K^\theta_{\mathrm{N-C-N}}$
334.72	125.52	146.44	292.88
$\phi_{\mathrm{H-N-C-O}}$ (degree)	$\phi_{\mathrm{H-N-C-O}}$ (degree)	$\phi_{\mathrm{N-N-C-O}}$ (degree)	$\phi_{\mathrm{C-H-N-H}}$ (degree)
180.0	0.0	180.0	180.0
$K^\phi_{\mathrm{H-N-C-O}}$	$K^\phi_{\mathrm{H-N-C-O}}$	$K^\phi_{\mathrm{N-N-C-O}}$	$K^\phi_{\mathrm{C-H-N-H}}$
10.46	8.37	43.93	4.60
q_{O} (e)	q_{C} (e)	q_{N} (e)	q_{H} (e)
-0.660	0.884	-0.888	0.388

Table 2.2: Improved GAFF parameters for urea.[23] The oxygen atom, carbon atom, hydrogen atoms, and nitrogen atoms are denoted by O, C, H, and N, respectively. The bond length is denoted by d, bond angle by θ, dihedral angle by ϕ, and the charges on the sites by q. The force constants, K^d are given in kJ mol^{-1} Å^{-2}, K^θ in kJ mol^{-1} radian^{-2}, and K^ϕ in kJ mol^{-1}.

2.4 Aspirin model

The unit cell representation of the aspirin crystal has been taken from a neutron diffraction study.[28] The unit cell was relaxed for the force field, and the modified lattice parameters[29] obtained from optimization of the bulk crystal structure were in good agreement with the experimental data. The molecular geometry of the aspirin molecule and the unit cell are displayed in Figure 2.3.

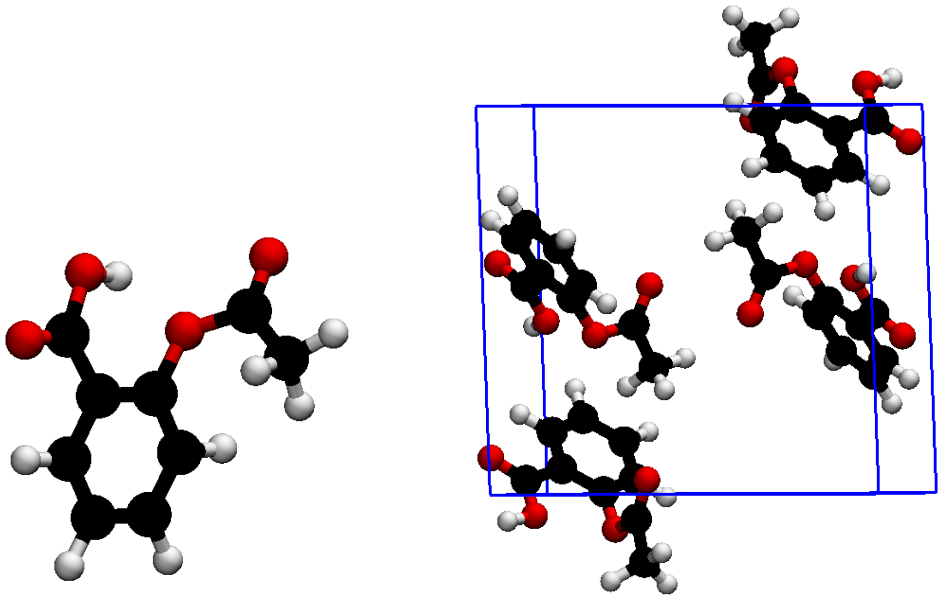

Figure 2.3: Geometrical representation of the aspirin molecule and the unit cell of aspirin crystal. The space group is $P21/c$. The modified lattice parameters are, $a = 1.140$, $b = 0.660$, $c = 1.150$ nm, and $\beta = 91.9$ degrees. The oxygen atoms are represented in red, hydrogen atoms in gray, and the carbon atoms in black.

2.5 Algorithms

In this section some of the methods used by GROMACS during the simulation of various systems are elucidated. First, the Molecular Dynamics(MD) algorithm is discussed, followed by the periodic boundary conditions, temperature and pressure coupling methods, and finally

the constraint algorithm is discussed in detail.

2.5.1 Molecular dynamics

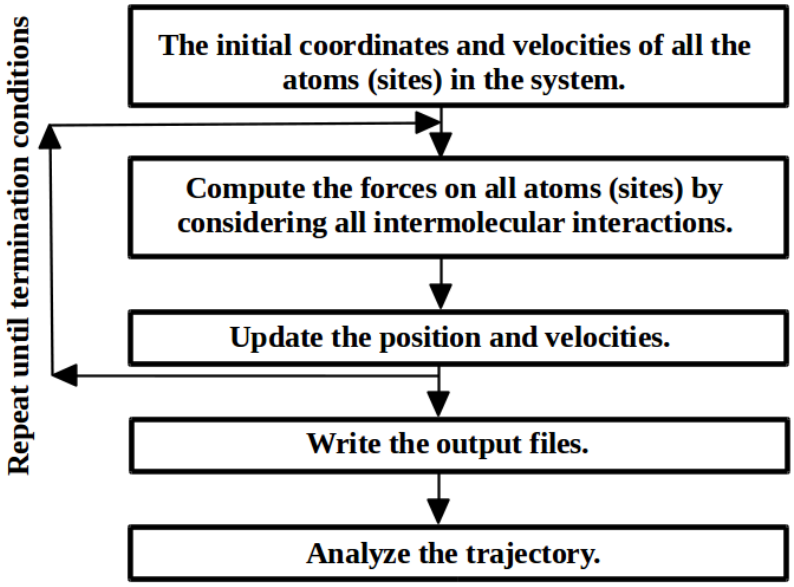

Figure 2.4: The basic Molecular Dynamics (MD) algorithm

Molecular dynamics is a computational method used to study the evolution of a N-body system. A schematic of the basic MD algorithm is displayed in Figure 2.4. The initial coordinates and the velocities (can also be generated by GROMACS) are specified as input, along with a description of the interatomic interactions and the system conditions under study. The initial states for simulation were generated using the models discussed in the Sections 2.2, 2.3, and 2.4. Initial configurations were obtained by placing the crystal at the center of a cubic simulation cell and the filling the cell with water molecules. The system is allowed to evolve in time and the trajectories are obtained by numerically solving Newton's equations of motion,

$$\boldsymbol{f_i} = m_i \ddot{\boldsymbol{r}}_{\boldsymbol{i}} \ , \tag{2.1}$$

where m_i is the mass of the corresponding interaction site, $\ddot{\boldsymbol{r}}_{\boldsymbol{i}}$ is the acceleration, and $\boldsymbol{f_i}$ is the total force experienced by site i. The trajectory, $\boldsymbol{r_i}(t)$, is obtained by numerically integrating

Newton's equations of motion, and can be used to calculate various dynamical and equilibrium properties of the system under investigation. The total force $\boldsymbol{f_i}$ on any site is computed by considering both bonded and non-bonded interactions plus any restraint or external force.

The method used to integrate the equations of motion is the leap-frog algorithm,[30] which updates the velocities and positions of the particles as follows:

$$\boldsymbol{r}_i(t + \Delta t) = \boldsymbol{r}_i(t) + \Delta t \boldsymbol{v}_i(t + \frac{\Delta t}{2}) \ , \tag{2.2}$$

$$\boldsymbol{v}_i(t + \frac{\Delta t}{2}) = \boldsymbol{v}_i(t - \frac{\Delta t}{2}) + \Delta t \boldsymbol{a}_i(t) \ , \tag{2.3}$$

$$\boldsymbol{a}_i(t) = \frac{\boldsymbol{f}_i(t)}{m_i} \ , \tag{2.4}$$

$$\boldsymbol{f}_i(t) = -\nabla u_i(\boldsymbol{r}_i) \ . \tag{2.5}$$

It can be noted that the positions and velocities are calculated at different time steps. A very small time step, Δt (1 femtosecond) has been chosen for all the simulations performed in this thesis.

The bonded interaction parameters (force constants) are included in the force field model and the bonds are constrained during the evolution of the system using the method described in section 2.5.4. The non-bonded interaction are modeled using the LJ and coulombic potentials, and are computed by considering a list of non-bonded atoms within a specified cutoff radius. The LJ potential consists of two terms, the r^{-12} term which is a repulsive term describing the short range repulsion due to overlapping electron orbitals, and the r^{-6} term which is an attractive term describing attraction at long range

$$u_{\mathrm{LJ}}(r_{ij}) = 4\epsilon_{ij} \left[\left(\frac{\sigma_{ij}}{r_{ij}} \right)^{12} - \left(\frac{\sigma_{ij}}{r_{ij}} \right)^{6} \right] \ , \tag{2.6}$$

where σ_{ij} and ϵ_{ij} are the LJ parameters for the sites under consideration, and r_{ij} is the interatomic distance. The Lorentz-Berthelot combining rules[31] are most often used to calculate

the LJ parameters for a pair of atoms from individual atom LJ parameters,

$$\sigma_{ij} = \frac{1}{2}\left(\sigma_i + \sigma_j\right) \quad , \tag{2.7}$$

$$\epsilon_{ij} = \left(\epsilon_i \epsilon_j\right)^{\frac{1}{2}} \quad , \tag{2.8}$$

where σ_i, σ_j, ϵ_i, and ϵ_j are the individual particle LJ parameters. The coulombic potential depends on the partial charges on the atoms, q_i and q_j, and the interatomic separation r_{ij},

$$u_{\mathrm{C}}(r_{ij}) = \frac{1}{4\pi\epsilon_0}\frac{q_i q_j}{r_{ij}} \quad , \tag{2.9}$$

where ϵ_0 is the permittivity of free space.

2.5.2 Periodic boundary conditions

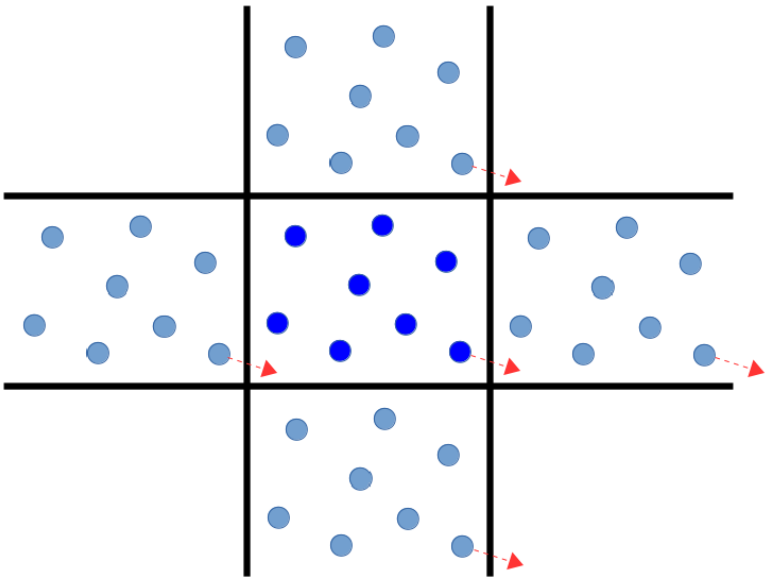

Figure 2.5: Periodic boundary conditions in two dimensions. The dark blue box is the central cell which is repeated in all directions.

There are various conditions that are employed to calculate bulk properties by using a small (finite) part of the whole (infinite) system. These conditions known as the periodic boundary

conditions (PBC), minimize the edge effects of the finite system under investigation. The PBC algorithm surrounds the finite box by translated copies of itself, as shown in Figure 2.5, and as the system evolves particles in all the boxes move in an identical manner. Thus, if a particle leaves the box at one end, an identical particle enters the box at the other end.

As a result of PBC, there is an enormous increase in the number of interacting pairs, as the particle not only interacts with other particles in the box but with their images. This problem is tackled by using a minimum image convention combined with a spherical cutoff, which only allows the nearest neighbors of particle images to interact.

The short-range interactions in the minimum image convention are calculated by considering the interaction of an atom with the nearest atom or image in the periodic system. If an atom leaves the box, the interaction calculation is done by considering the incoming image. The cutoff for short-range interactions is restricted to half the box length, which can be significantly bigger than the cutoff for the potential used (of the order of ∼1 nm).

The long-range electrostatic forces have ranges greater than half the box length and are thus harder to treat. The total electrostatic energy of an atom in the central box can be written as

$$u_i = \frac{1}{4\pi\epsilon_0} \sum_{\boldsymbol{n}} \sum_{j}^{N}{}' \frac{q_i q_j}{r_{ij,\boldsymbol{n}}} \quad , \tag{2.10}$$

where $\boldsymbol{n} = (n_x, n_y, n_z)$ is the box index vector, $r_{ij,\boldsymbol{n}}$ is the actual distance between the charges and the prime indicates that $i \neq j$ when $\boldsymbol{n} = \{0\}$. The sum in Equation (2.10) is conditionally convergent which is troublesome and a number of methods have been proposed to tackle this problem.

The Ewald summation[32] is a technique that is used to calculate the long-range interactions. It basically converts the single long-ranged term into two short-ranged terms (one in real space and the other in reciprocal space) and a constant term. The expression for the electrostatic energy after using Ewald summation can be written as

$$u_i = u_i^S + u_i^L + u_i^{self} \quad , \tag{2.11}$$

$$u_i^S = \frac{1}{4\pi\epsilon_0}\frac{1}{2}\sum_{\boldsymbol{n}}\sum_{j}^{N}{}' \frac{q_i q_j}{r_{ij,\boldsymbol{n}}}\mathrm{erfc}\left(\frac{r_{ij,\boldsymbol{n}}}{2^{\frac{1}{2}}\sigma}\right) \quad , \tag{2.12}$$

$$u_i^L = \frac{1}{2V\epsilon_0}\sum_{\boldsymbol{k}\neq\boldsymbol{0}}\sum_{j}^{N}\frac{q_i q_j}{k^2}\exp^{\iota\boldsymbol{k}.\boldsymbol{r_{ij}}}\exp^{-\sigma^2k^2/2} \quad , \tag{2.13}$$

$$u_i^{self} = -\frac{1}{4\pi\epsilon_0}\frac{1}{(2\pi)^{\frac{1}{2}}\sigma}q_i^2 \quad , \tag{2.14}$$

where $\mathrm{erf}(z) = \frac{2}{\pi^{1/2}}\int_0^z \exp^{-t^2}\,dt$, $\mathrm{erfc}(z) = 1 - \mathrm{erf}(z)$, V is the volume of the cell, $k = |\boldsymbol{k}|$, $\boldsymbol{k}$ is the reciprocal lattice vector, and σ is the standard deviation of the Gaussian distribution which is used to modulate the convergence rate. The first term in Equation (2.11), u_i^S is similar to the total interaction energy u_i, and can be truncated at a certain cutoff due to inclusion of the $\mathrm{erfc}(r)/r$ term, which decays very rapidly with r. The second term u_i^L is the sum of the long-range potential in reciprocal space, and u_i^{self} is the self interaction term, to negate the extra term added in the second term u_i^L, to include the potential generated by the site i itself.

The classical Ewald method scales as $\mathcal{O}(N^2)$, while the variant particle mesh Ewald[33] (PME) method is an advanced method using the fast Fourier transform[34] technique to compute the reciprocal term, which scales as $\mathcal{O}(N\log(N))$, where N is the number of charges. Thus the PME method is most commonly used as it is more efficient.

2.5.3 Temperature and pressure control

The molecular dynamics algorithm discussed in Section 2.5.1 gives rise to the NVE (constant number of particles, volume, and energy) ensemble. However, most of the quantities we wish to calculate are at fixed temperature and pressure, which cannot be well controlled by using the above algorithm. So, we now discuss various methods that are used to control the temperature and pressure of a system during a simulation.

Nosé-Hoover thermostat

The instantaneous temperature of a system of N particles is related to the kinetic energy

of the system $\mathcal{K}$ by

$$T = \frac{2\mathcal{K}}{k_{\mathrm{B}} N_f} \ , \tag{2.15}$$

where N_f is the total number of degrees of freedom. The Nosé-Hoover thermostat[35,36] introduces terms representing a thermal reservoir into the system Hamiltonian and a dynamic parameter ξ, whose physical meaning is that of a friction which accelerates or decelerates the particles until the temperature is equal to the desired value. The final Hamiltonian of the system after inclusion of the parameter is

$$H = \mathcal{K} - \mathcal{V} + \frac{p_\xi^2}{2Q} + N_f k_B T_0 \xi \ , \tag{2.16}$$

where p_ξ is the conjugate momentum of the friction parameter, and $\mathcal{K}$ and $\mathcal{V}$ are the kinetic and potential energies of the system of N particles, respectively. The last two terms in Equation (2.16) can be interpreted as the kinetic and potential energy associated with a thermal reservoir. The equations of motion are modified to

$$\ddot{\boldsymbol{r}}_{\boldsymbol{i}} = \frac{\boldsymbol{F_i}}{m_i} - \frac{p_\xi}{Q} \dot{\boldsymbol{r}}_{\boldsymbol{i}} \ , \tag{2.17}$$

$$\frac{\mathrm{d}p_\xi}{\mathrm{d}t} = \sum_i^N m_i \frac{v_i^2}{2} - \frac{N_f + 1}{2} k_B T_0 \ , \tag{2.18}$$

where T_0 is the target temperature and Q is a mass parameter which along with the target temperature determines the strength of the coupling. The mass parameter Q is related to the target temperature T_0 by

$$Q = \frac{\tau_T^2 T_0}{4\pi^2} \ , \tag{2.19}$$

where τ_T is the period of oscillation of kinetic energy between the system and the reservoir, and is a better parameter to control the coupling strength, because it is independent of the system size and target temperature.

Parinello-Rahman barostat

The Parinello-Rahman barostat[37] like the Nosé-Hoover thermostat modifies the equations

of motion to allow the box vectors to evolve in time to produce the desired pressure. The box vectors $\boldsymbol{a}$, $\boldsymbol{b}$ and $\boldsymbol{c}$ are time dependent and are represented by a matrix $\boldsymbol{h} = \{\boldsymbol{a}, \boldsymbol{b}, \boldsymbol{c}\}$. The volume of the box V is then defined as: $V = \det(\boldsymbol{h}) = \boldsymbol{a} \bullet (\boldsymbol{b} \times \boldsymbol{c})$, where the dot represents a scalar product. The Lagrangian of the system subjected to an external pressure p can be written as

$$\mathcal{L} = \mathcal{K} - \mathcal{V} + \frac{1}{2} M \mathrm{Tr}(\dot{\boldsymbol{h}}' \dot{\boldsymbol{h}}) - pV \ , \tag{2.20}$$

where the prime denotes the transpose, and $\mathcal{K}$ and $\mathcal{V}$ are the kinetic and potential energy of the system of N particles, respectively. The last two terms in Equation (2.20) can be interpreted as the kinetic and potential energies associated with a piston applying an external pressure. The coordinates of the particles are now represented as

$$\boldsymbol{s_i} = \mathbf{h^{-1}} \boldsymbol{r_i} \ , \tag{2.21}$$

and the equation of motion is modified to

$$\ddot{\boldsymbol{s}}_{\boldsymbol{i}} = -\sum_{j \neq i} \frac{\mathrm{d}u}{\mathrm{d}r_{ij}} \frac{1}{m_i r_{ij}} (\boldsymbol{s_i} - \boldsymbol{s_j}) - G^{-1} \dot{G} \dot{\boldsymbol{s}}_{\boldsymbol{i}} \ , \tag{2.22}$$

$$\ddot{\mathbf{h}} = \frac{1}{M} (\boldsymbol{\pi} - p) \boldsymbol{\sigma} \ , \tag{2.23}$$

where the terms $\boldsymbol{\pi}$, the microscopic stress tensor, $\boldsymbol{\sigma}$, a matrix containing the direction of the reciprocal vectors and G, known as the metric stress tensor are defined as follows:

$$V\boldsymbol{\pi} = \sum_i m_i \boldsymbol{v_i} \boldsymbol{v_i}' - \sum_i \sum_{j>i} \frac{\mathrm{d}u}{\mathrm{d}r_{ij}} \frac{1}{r_{ij}} \boldsymbol{r_{ij}} \boldsymbol{r_{ji}}' \ , \tag{2.24}$$

$$\boldsymbol{\sigma} = \{\mathbf{b} \times \mathbf{c}, \mathbf{c} \times \mathbf{a}, \mathbf{a} \times \mathbf{b}\} \ , \tag{2.25}$$

$$G = \mathbf{h}' \mathbf{h} \ . \tag{2.26}$$

2.5.4 Constraint algorithm

In a molecular dynamics simulation, the sites move around under the influence of intermolecular forces affecting the geometry (chemical bonds and bond angles) of some molecules. Thus we need to apply certain constraints on every molecule to conserve the molecular geometry during the evolution. In this section we discuss the linear constraint solver (LINCS)[38] algorithm which is a method that resets the bonds to their correct lengths in two steps, an unconstrained evolution and a projection of the new bonds on the old ones.

The system is constrained using a set of k time independent equations

$$g_i(\boldsymbol{r}) = |\boldsymbol{r}_{i_1} - \boldsymbol{r}_{i_2}| - d = 0, \qquad i = 1, 2, ...k \ , \tag{2.27}$$

$$\boldsymbol{r} = \{\boldsymbol{r_1}, \boldsymbol{r_2}.....\boldsymbol{r_N}\} \ , \tag{2.28}$$

where d is the length of the bond between atoms i_1 and i_2. These holonomic constraints (dependent only on position $\boldsymbol{r}$ and time t) are included in the Lagrangian as

$$\mathcal{L} = \mathcal{K} - \mathcal{V} + \boldsymbol{\lambda} \bullet \boldsymbol{g} \ , \tag{2.29}$$

where $\boldsymbol{\lambda} = \{\lambda_1, ...\lambda_k\}$ are the k Lagrange multipliers associated with the constraints $\boldsymbol{g} = \{g_1, ...g_k\}$, and $\mathcal{K}$ and $\mathcal{V}$ are the kinetic and potential energies of the system. The resulting equations of motion can be expressed as

$$\ddot{\boldsymbol{r}} = (\mathbf{I} - \mathbf{TB})\mathbf{M^{-1}f} - \mathbf{T}\dot{\mathbf{B}}\dot{\mathbf{r}} \ , \tag{2.30}$$

$$\mathbf{T} = \mathbf{M^{-1}B'}(\mathbf{BM^{-1}B'}) \ , \tag{2.31}$$

where the prime and dot represent the transpose and derivative with respect to time, respectively, $\mathbf{M} = \mathrm{diag}(m_1, m_1, m_1, ...m_N, m_N, m_N)$ is a $3N$ dimensional diagonal matrix containing the masses of the particles, and $\mathbf{B}$ is a K $\times$ $3N$ matrix, containing the directions of the

constraints

$$B_{hi} = \frac{\partial g_h}{\partial r_i} \ . \tag{2.32}$$

$\mathbf{I - TB}$ is a projection matrix, $\mathbf{M^{-1}f}$ is the acceleration vector, and the last term in Equation (2.30) represents centripetal forces caused by rotation of bonds. The LINCS algorithm can be easily implemented by first using the leap-frog algorithm to find the unconstrained positions and velocities ($\boldsymbol{r}^*$ and $\boldsymbol{v}^*$), and then projecting them to conserve the constraints as follows:

$$\boldsymbol{r}(t + \Delta t) = (\mathbf{I - TB})\boldsymbol{r}*(t + \Delta t) + \mathbf{Td} \ , \tag{2.33}$$

$$\boldsymbol{v}(t + \frac{\Delta t}{2}) = (\mathbf{I - TB})\boldsymbol{v}*(t + \frac{\Delta t}{2}) + \frac{1}{\Delta t}\mathbf{T}(\mathbf{Br - d}) \ , \tag{2.34}$$

where the terms $\mathbf{Td}$ and $\frac{1}{\Delta t}\mathbf{T}(\mathbf{Br - d})$ are position and velocity correction terms added to the equations to prevent accumulation of numerical error in computer implementation,[38] and $\mathbf{d}$ is a vector containing the bond lengths.

Chapter 3

Dissolution of Urea Nanocrystals

3.1 Overview

Molecular dynamics simulations are used to determine the mechanism of urea crystal dissolution in water under sink conditions. Crystals of cubic and tablet shape are considered, and results are reported for four commonly used water models. The dissolution rates for the different water models differ considerably, but the overall dissolution mechanism remains the same. Urea dissolution occurs in three stages: a relatively fast initial stage, where molecules leave high energy sites such as corners and edges, a slower intermediate stage during which the bulk of the crystal dissolves, and a final stage where the small crystal remnant looses its structure and completely disintegrates. We show that during the long intermediate stage the dissolution process is well described by a simple classical model which assumes that the dissolution rate is proportional to the active surface area. The active surface area is a region of the crystal surface from which molecules leave uniformly after the initial stage of dissolution. For initially cubic and tablet-shaped crystals the active surface areas are spherical and cylindrical, respectively, and the corresponding integrated rate laws give excellent fits to the simulation results. By carrying out simulations at different temperatures we show that urea dissolution is an activated process, the rate constants obey the Arrhenius equation with an activation energy of ~ 32 kJ mol^{-1} for a cubic crystal. Our simulations give no indication of a significant diffusion layer, and we conclude that the detachment of urea molecules from the crystal surface is the rate determining step in the dissolution process. We note that the dissolution mechanism, and the applicability of classical rate laws, that we report for urea are consistent with earlier observations for the dissolution of NaCl crystals.[6] This suggests that

the three-stage mechanism and classical rate laws might also apply to the dissolution of other ionic and molecular crystals.

3.2 Introduction

Molecular solids are an important class of compounds of relevance in the pharmaceutical and special chemicals industries, among other applications.[12,13,39–44] The dissolution of solids is a crucial process in many physical systems and situations.[12,13] Given this, crystal dissolution has been a subject of interest for the past century,[10,45] with current research strongly focussed on gaining a detailed understanding of dissolution at the molecular level.[14]

In principle, computer simulations employing molecular dynamics (MD) or other methods provide an ideal approach to gaining a microscopic understanding of dissolution. However, in practice, until recently this method has not been widely exploited due partially to the complex nature of interesting molecules, and because the large amounts of simulation time required exceeded the power of most computational facilities. However, during the past few years simulations of dissolution have become feasible due to great increases in computing power, and to the ever evolving development of accurate forcefields for complex molecules. We note that the last point is particularly important in the dissolution context, since to be useful in dissolution studies a model must give a good representation of both solution and solid properties.

Despite the potential issues, there have been several recent investigations of dissolution employing simulation methods.[6,15–17] We note in particular the work of Gao and Olsen[16] which revealed the importance of edges and corners as the sites from which molecules initially detach from a crystal. In another important study, Elts et al.[17] have proposed a simulation approach that combines MD and kinetic Monte Carlo methods, such as to overcome the long simulation times required for the dissolution of some crystals. They applied their techniques in a detailed study of aspirin dissolution in water, and reported a dissolution mechanism in good accord with experimental observation.

In a recent paper, Patey and Lanaro[6] employed direct MD simulations to investigate the complete dissolution of differently shaped NaCl nanocrystals. For model NaCl, dissolution is sufficiently fast that the dissolution process can be followed until an entire crystal has dissolved. An interesting finding of this work was that NaCl dissolution essentially occurs in three stages, a relatively fast initial stage where particles are removed from high energy sites (mainly edges and corners, depending on the initial crystal shape), a long slower intermediate stage where dissolution closely follows a fixed rate law, and a final stage where crystalline order is lost as the dissolution process is completed. Additionally, it was shown that during the intermediate stage which dominates the dissolution process, the dissolution rate is well described by classical models,[1–5,46,47] which take account of the varying surface area of the crystal as it dissolves. Ion detachment from the NaCl crystal is the rate determining step, and the particular form of the integrated rate law depends on the initial crystal shape.

The purpose of the present chapter is to examine if, and to what extent, the rather simple three-stage dissolution process found for NaCl holds for molecular solids. To do this, we examine the complete dissolution of urea nanocrystals in water under so-called sink conditions, where the solution concentration at complete dissolution is much less than saturation. We note that there have been many simulation studies of model aqueous urea solutions,[15,48–50] and that Piana and Gale[15] have examined both crystallization and dissolution of urea in aqueous systems. However, while their work is interesting, Piana and Gale only considered systems where a single urea surface (001) was in contact with water, and do not address the stages of dissolution, and the shape-dependent rate laws in which we are interested.

We selected urea for this investigation for several reasons. Firstly, as noted above, a study of this type requires a forcefield which gives a good description of both crystalline and solution phases. As discussed in Section 3.3, this is not true of all common urea models, but there is at least one urea model which satisfies both conditions. Secondly, at ambient temperatures, the dissolution of urea occurs sufficiently fast that nanocrystals ($\sim$ 1000 urea molecules) can be completely dissolved on feasible simulation time scales, allowing us to follow the complete dissolution process. Finally, urea is a molecule of importance in many physical systems.[51–53]

In this chapter, we examine the dissolution of both cubic and tablet-shaped urea nanocrystals at temperatures ranging from 300 to 340 K. Four different water models are considered, and, although the observed dissolution processes are qualitatively similar, some significant quantitative differences do occur. Our main finding is that the dissolution of urea crystals follows a pattern that is very similar to that observed for NaCl, with simple rates laws giving a good description of the important intermediate stage of dissolution. Our analysis of rate laws and the activation energy indicates that detachment of urea molecules from the crystal is the rate determining step in the dissolution process.

The remainder of the chapter is organized into three sections. The models and methods are described in Section 3.3, a detailed description of our findings is given in Section 3.4, and our conclusions are summarized in Section 3.5.

3.3 Models and methods

In the present simulations all site-site pair interactions, $u(r_{ij})$, consist of Lennard-Jones (LJ) plus Coulombic terms such that

$$u(r_{ij}) = 4\epsilon_{ij}\left[\left(\frac{\sigma_{ij}}{r_{ij}}\right)^{12} - \left(\frac{\sigma_{ij}}{r_{ij}}\right)^{6}\right] + \frac{1}{4\pi\epsilon_0}\frac{q_i q_j}{r_{ij}}, \tag{3.1}$$

where q_i and q_j are charges on sites i and j, r_{ij} is the distance between sites i and j, σ_{ij} and ϵ_{ij} are the LJ length and energy parameters, and ϵ_0 is the permittivity of free space.

During the past few decades a number of different atomistic models for urea have been proposed.[22] For example, the OPLS/GROMOS[54,55] model for urea has been widely employed in simulations of aqueous solutions. However, we found that with this model urea nanocrystals were not stable under ambient conditions.

In order to investigate urea dissolution, we need a model that produces stable nanocrystals of urea. The best model available for this purpose appears to be the the Generalised AMBER Force Field (GAFF),[23] which has been shown to give stable urea nanocrystals, and a good description of the properties of crystalline urea.[24] The GAFF potential parameters are given

in Table 3.1. The GAFF parameters are used to generate an AMBER topology file, which is then converted to GROMACS topology for simulations. Several different water models have been used in studies involving urea in aqueous solution.[15,22,50] Among others, these include the SPC,[18] SPC/E,[19] TIP3P,[20] and TIP4P[56] water models. In the present chapter we carry out simulations with the SPC, SPC/E, TIP3P, and TIP4P/2005[21] models to investigate any dependence on the particular water model employed. We note that, of all the rigid water models available, TIP4P/2005 gives the best overall agreement with experimental results for pure water.[57] For all models the usual Lorenz-Berthelot combining rules[31] were used in the calculation of the LJ interactions.

	σ(Å)	ϵ(kJ mol^{-1})	q(e)
C	1.9080	0.3598	0.884
O	1.6612	0.8786	-0.660
N	1.8240	0.7113	-0.888
H	0.6000	0.0657	0.388

Table 3.1: The GAFF LJ parameters and partial charges for urea[23]

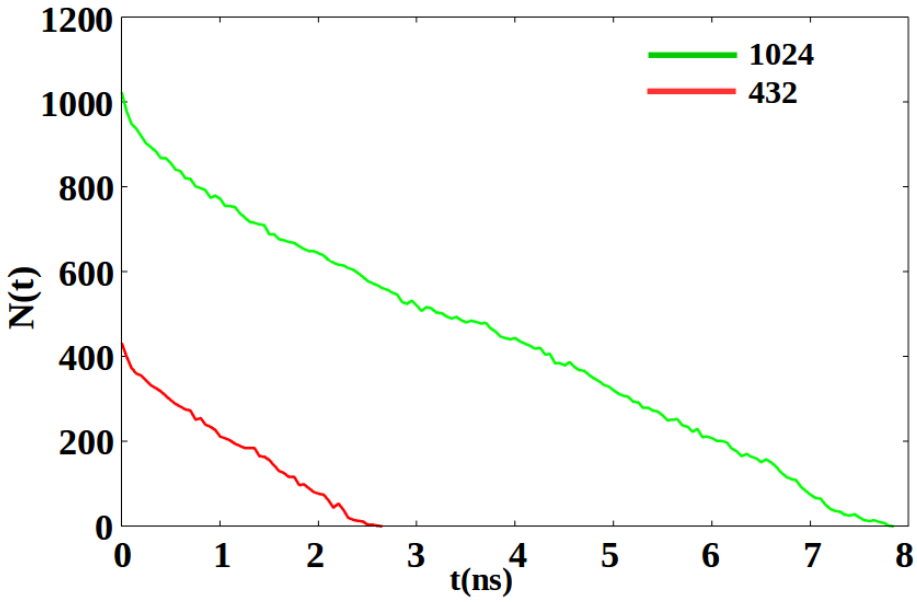

Figure 3.1: Dissolution profiles obtained with the SPC water model for cubic crystals of different size (1024 and 432 molecules), plotted as the number of molecules in the crystal vs time.

Simulations were carried out for urea nanocrystals shaped as cubes and as tablets, in order to examine the influence of shape on the dissolution process. The cubic crystals consisted of 1024 urea molecules, and were constructed by repeating the urea unit cell[26] eight times in each direction. In order to ensure that our conclusions on dissolution are not strongly dependent on the crystal size, a test simulation using SPC water was performed with a crystal of 432 molecules at 300 K. The results were qualitatively similar to those obtained with 1024 molecules as can be seen in the Figure 3.1. Tablet-shaped crystals contained 1264 molecules, and were generated by repeating the unit cell 16, 16, and 4 times along the crystal axes, and then removing all molecules that were outside a circle of 4 nm centered on the axis of the cylinder. Configurational snapshots of both cubic and tablet-shaped crystals are given below (see Figures 3.4 and 3.7).

The experimental saturation concentrations[48] of urea for our simulation conditions correspond to urea mole fractions in the range $0.26 - 0.43$. All simulations were carried out at urea mole fractions that were less than 0.035, or at concentrations less than one eighth of the experimental saturation concentrations. We would expect these concentrations to meet the so-called sink condition, which refers to solutions where the concentration is so low that molecular reattachments do not significantly influence the dissolution rate.[58] We tested that sink conditions were indeed met for our model system by carrying out simulations at different concentrations, as discussed in Section 3.4. The numbers of urea and water molecules included in each simulation, together with the temperatures considered, are summarized in Table 3.2.

	Urea	Water		Models		Temp(K)
		SPC	SPC/E	TIP3P	TIP4P/2005	
Cube	1024	29873	29873	29873	30125	300
	1024	29873	29873	29873	30125	320
	1024	29873	29873	29873	30125	340
	1024	40576	n/a	n/a	n/a	300
Tablet	1264	39672	n/a	n/a	n/a	300

Table 3.2: A summary of the numbers of urea and water molecules used, the shapes of the initial crystals, and the temperatures at which simulations were performed.

All simulation were carried out under NPT conditions at a pressure of 1 bar, using the

GROMACS[59] molecular dynamics package, version 4.5.5. The temperature was controlled using the Nosé-Hoover thermostat[35,36] with a time constant of 2.0 ps, and the pressure was maintained by means of the Parrinello-Rahman barostat,[37] with a compressibility of 4.46×10^{-5} bar^{-1} and a time constant of 2.0 ps. The time step used for all simulations was 1 fs. Periodic boundary conditions were applied, and the short-range interactions were truncated at 1 nm. The electrostatic interactions were taken into account using the fourth order particle mesh Ewald method[33] with a Fourier spacing of 0.12 nm. All bonds were constrained using the LINCS algorithm.[38]

Initial configurations were obtained by placing the urea crystal at the center of the cubic simulation cell, and the filling the cell with water molecules. Water molecules located too close to the surface of the crystal (within 0.1 nm) were removed. The system was then relaxed for a brief period, keeping the urea molecules fixed, so as to remove any gaps occurring at the crystal-water interface due to the removal of water molecules. The system was then evolved in time until complete dissolution of the crystal. This process took times ranging from 2.10 ns to 12.05 ns, depending on the temperature of the system.

In order to identify urea molecules as solution or crystal molecules, an order parameter based on counting the number of neighboring urea molecules was used. The number of neighbors of a molecule in the crystal is substantially higher than that of a molecule in solution, and this difference was used to devise a simple order parameter for classification. For this purpose, the number of neighbors is defined as the number of molecules within a sphere of radius 0.6 nm, centered at the center of mass of the molecule. The number of urea neighbors of a molecule in the crystal lies in the range $12 - 14$, and that of a molecule in the solution is in the range $0 - 2$. Therefore, we chose 7 neighbors as a cutoff value, any molecule with fewer than 7 neighbors is considered to be part of the solution, and those with 7 or more neighbors are considered to be part of the crystal. The simulation results were not very sensitive to the exact value of the cutoff, similar dissolution profiles were for cutoffs ranging from 6 to 8 neighbors.

3.4 Discussion

3.4.1 Dissolution profiles

Cubic crystals

Dissolution profiles for an initially cubic urea crystal at 300 K are plotted in Figure 3.2. Results are included for all four water models, and we see some significant model dependence. The time required for complete dissolution varies from ~ 7 ns in the fastest case (TIP3P) to ~ 11 ns in the slowest (SPC/E), with SPC and TIP4P/2005 both taking ~ 8 ns. For all four models the initial conditions were very similar, and consistent model differences occurred in different simulation runs, and at different temperatures. Note that profiles for two simulations with SPC/E water with different initial conditions are included in Figure 3.2, and that only small differences are observed. Therefore, the discrepancies apparent in Figure 3.2 reflect a real dependence on the water model employed. A further discussion of the model dependence is given below, where we consider the temperature dependence and activation energies (Section 3.4.2).

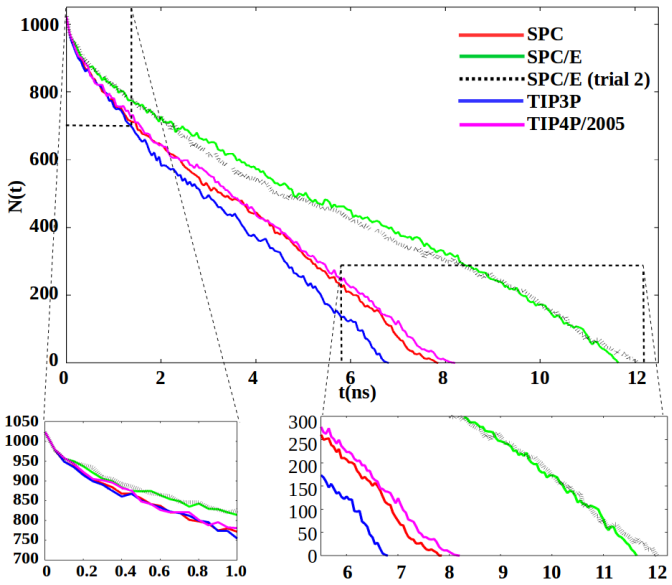

Figure 3.2: Dissolution profiles for cubic crystals obtained with different water models. $N(t)$ is the number of molecules in the crystal at time t. Note that results from two simulation runs are shown for the SPC/E model.

In order to be certain that we are truly under sink conditions and that finite solution concentration is not influencing our results, we carried out two simulations (using SPC water) at mole fractions of 0.03428 and 0.02561 (calculated at complete dissolution), keeping all other conditions fixed. The dissolution profiles are shown in Figure 3.3, and we see that no significant differences are observed, confirming that we are indeed in the sink regime.

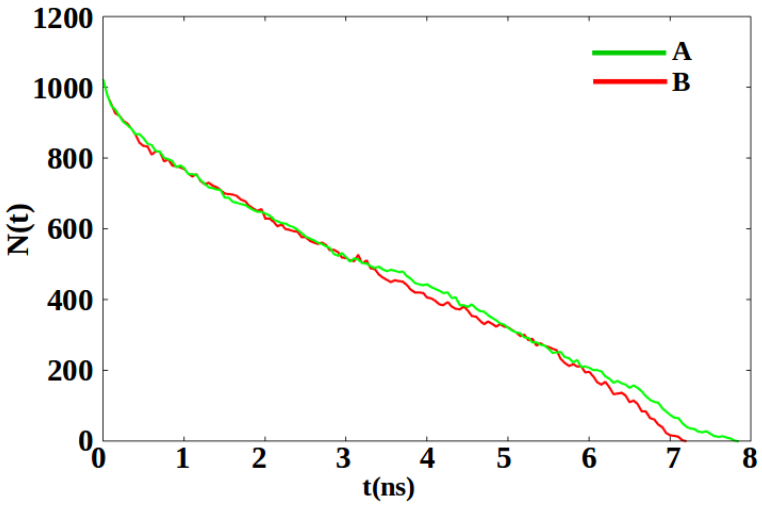

Figure 3.3: Simulations at different concentrations using the SPC water model. Curves A and B are for urea mole fractions of 0.03428 and 0.02524 (calculated assuming complete dissolution of the entire crystal). Note that there is no significant concentration effect.

Despite the water model dependence of the overall dissolution rate, by closely examining dissolution profiles, together with configurational snapshots, we determine that for all water models the urea dissolution process can be divided into three stages, that are similar to those previously observed[6] for the ionic crystal NaCl. An initial stage, where molecules are detached from the edges and corners of the crystal, followed by an intermediate regime where the crystal dissolves according to a fixed rate law, after it has lost its corners and edges, and a final stage where the solid looses its crystalline structure and completes its dissolution. The following is a more detailed discussion of the three dissolution stages.

During the initial stage of dissolution water molecules interact with the loosely bound molecules generally located on edges and corners of the urea crystal, and these molecules are

quickly dissolved. Following these rapid detachments, the active surface of the crystal further anneals such as to reduce the surface contact area for a crystal of given size. Configurational snapshots of a cubic crystal at various points on the dissolution curve are shown in Figure 3.4. The snapshots shown were obtained with the SPC water model, but the particular water model used does not change the qualitative nature of the dissolution process.

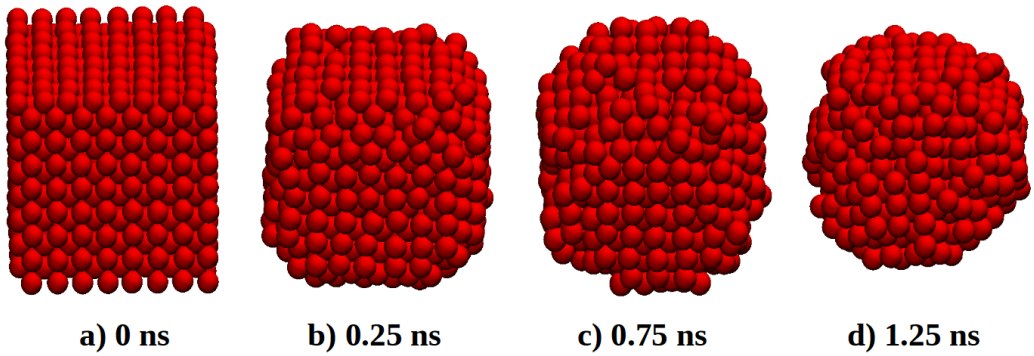

Figure 3.4: Configurational snapshots corresponding to different points in the dissolution profile of a cubic crystal in SPC water. Each red sphere indicates a urea molecule.

From the dissolution profiles shown in Figure 3.2 (note the magnification of the initial stage), we see that the initial slopes (between 0 and ~ 0.25 ns) are quite steep, after which the slopes decrease and remain roughly constant throughout the stage we refer to as the fixed rate law regime. During the rapid initial stage ~ 150 urea molecules ($\sim 14\%$) leave the crystal and enter the solution. It is evident from the snapshots in Figure 3.4 that these molecules leave the edges and corners of the crystal. After the initial period more molecules detach from the crystal, and this continues until the crystal is nearly spherical in shape, as can be seen in Figure 3.4(d). Once the crystal attains a spherical shape, the molecules leave the surface essentially uniformly, thus entering the fixed rate law regime. This regime continues until the final stage of dissolution (approximately the last nanosecond of the profiles shown in Figure 3.2), when the solid loses its crystalline order, becoming an amorphous urea cluster which continues to disperse into solution until no crystal remnant remains. This is illustrated in the configurational snapshots shown in Figure 3.5.

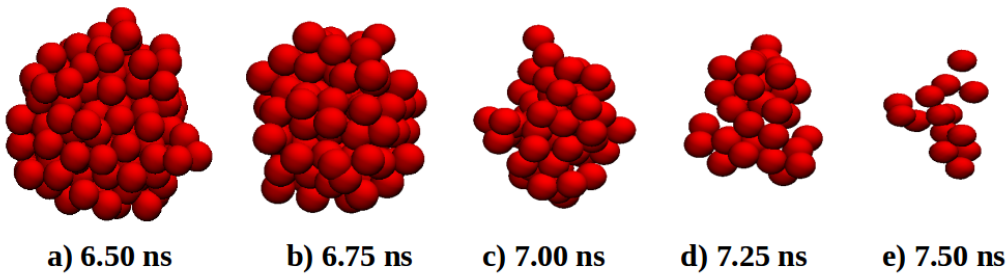

Figure 3.5: Configurational snapshots of the last stages in the dissolution profile of the cubic crystal in SPC water. Each red sphere indicates a urea molecule.

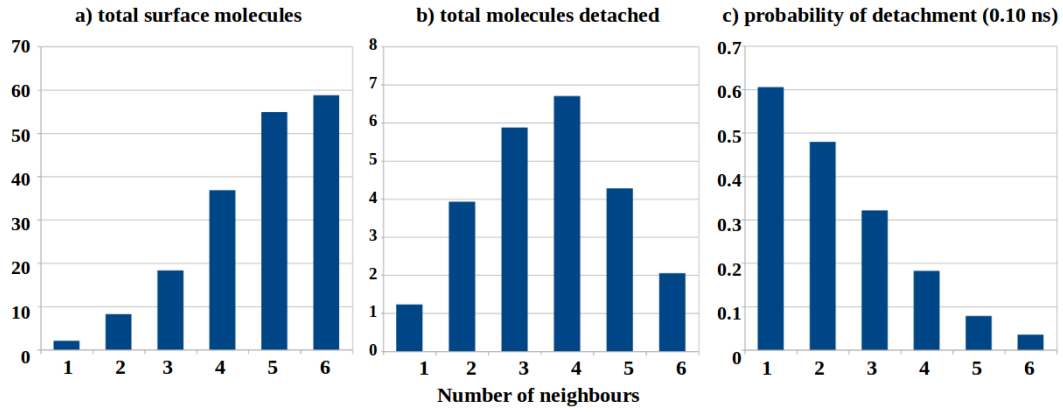

Figure 3.6: Quantities obtained as described in the text for a cubic crystal in SPC water. All quantities are plotted as functions of the number of urea neighbors in the first coordination shell. The results were obtained over the time interval 1 - 3 ns of a dissolution run.

To gain further insight into the influence of local environment on urea detachment from the crystal, we calculated the probability of detachment during a given time interval of surface molecules with different numbers of urea molecules in the first coordination shell. The first coordination shell is defined by a sphere of radius 0.5 nm centered at the molecular center of mass. The radius of the first coordination shell was selected based on the urea carbon-carbon radial distribution function. Surface molecules were identified as crystal molecules (defined as described in Section 3.3) having $1-6$ urea molecules in their first coordination shell. The number of molecules that detached from the crystal within 0.1 ns was recorded, and averages

were taken over 40 equally spaced time slices between 1 and 3 ns of a dissolution run. The calculation was started at 1 ns to ensure that the results were not influenced by the initial structure of the surface. The results obtained with SPC water are shown in Figure 3.6, and we see that the probability of detachment decreases dramatically as the number of neighbors increases, as one might expect. We note that the the particular time interval considered is not an important factor, results obtained using longer time intervals (0.15 ns and 0.2 ns) were qualitatively similar to those shown in Figure 3.6.

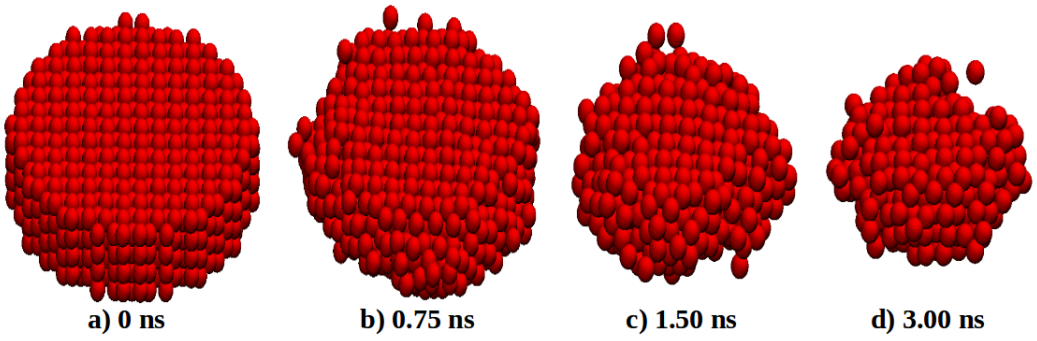

Figure 3.7: Configurational snapshots corresponding to different point in the dissolution profile of a tablet-shaped crystal in SPC water. Each red sphere indicates a urea molecule.

Influence of crystal shape

In order to investigate the possible influence of crystal shape, we also consider a tablet-shaped crystal, as depicted in Figure 3.7. A dissolution profile for the tablet obtained with SPC water is shown in Figure 3.8, and compared with the corresponding result for a cubic crystal. Since the numbers of molecules initially in the tablet-shaped and cubic crystals differ a little (Table 3.2), in Figure 3.8 we plot the fraction of molecules in the crystal, $f_{cry}(t) = N(t)/N_0$, where $N(t)$ is the number of molecules in the crystal at time t and N_0 is the initial number of molecules in the crystal. From Figure 3.8 we see that both tablet-shaped and cubic crystals have similar dissolution profiles, with an initial steep slope followed by a nearly constant dissolution rate. The initial slope for the tablet-shaped crystal can be explained by the fact that the weakly attached molecules at the edges of the tablet leave very quickly. Also,

molecules do not leave from the flat surface of the tablet, but only from the curved surface, such that the cylindrical shape of the crystal remains intact throughout the dissolution, as can be seen from the configurational snapshots in Figure 3.7. After the initial stage, the tablet dissolves at a faster rate than the cubic crystal. This can be attributed to the fact that the number of layers in the tablet is half the number in the cubic crystal. Thus, molecules on the active surface (the sides) of the tablet interact more weakly with the bulk crystal than molecules on the active surface (spherical) of the initially cubic crystal.

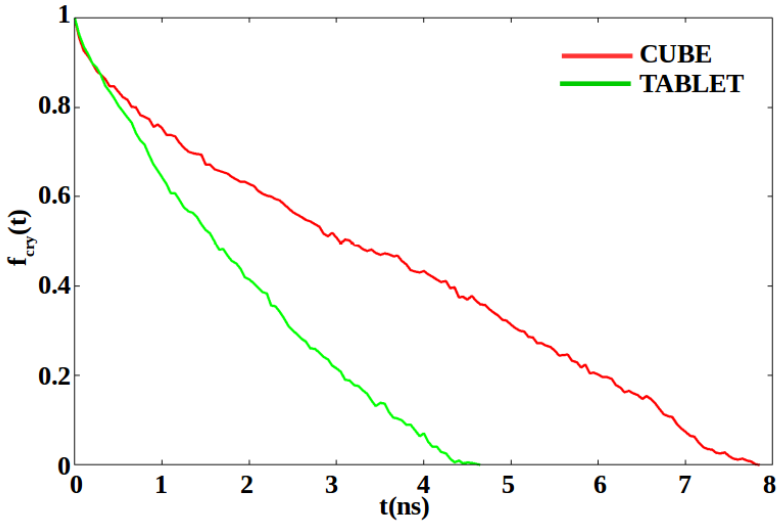

Figure 3.8: Comparison of the dissolution profiles of cubic and tablet-shaped crystals in SPC water. $f_{\mathrm{cry}}(t)$ is the fraction of molecules remaining in the crystal.

Comparison with dissolution models

As noted above, dissolution processes have been studied for over a century, and several possible rate laws have been proposed.[10,14] In earlier work[6] on the dissolution of NaCl crystals, we showed that a relatively simple rate law does indeed give a good description of dissolution in the fixed rate law regime, and it is interesting to check if this is also the case for urea. Under sink conditions we might expect the detachment process to be rate determining, such that the dissolution rate could be described by

$$\frac{dN(t)}{dt} = -kS_{\text{active}}(t) \ , \tag{3.2}$$

where $N(t)$ is the number of molecules in the crystal at time t, $S_{\text{active}}(t)$ is the active surface area from which detachments occur, and k is a rate constant. This law, which takes account of the changing surface area, was first suggested by Brunner and Tolloczko.[2]

Integrated rate laws can be obtained by identifying different forms for $S_{\text{active}}(t)$ and integrating eq 3.2. Noting that the active surface areas in the fixed rate law regime are approximately spherical and cylindrical for the cube and tablet, respectively, functional forms for $S_{\text{active}}(t)$ can be obtained by considering surface area to volume relationships. This gives $S_{\text{active}}(t) \propto N^{2/3}(t)$ for the cube and $S_{\text{active}}(t) \propto N^{1/2}(t)$ for the tablet, and the corresponding integrated rate laws

$$\sqrt[3]{N(t)} = \sqrt[3]{N_0} - kt, \qquad \text{(cube)}, \tag{3.3}$$

$$\sqrt{N(t)} = \sqrt{N_0} - kt, \qquad \text{(tablet)}, \tag{3.4}$$

where N_0 is the number of molecules in the crystal at $t = 0$, and k will obviously be different for each rate law.

			Cube		Tablet
	SPC	SPC/E	TIP3P	TIP4P/2005	
linear	0.98839	0.98244	0.98227	**0.99435**	0.98561
cube root	0.99068	**0.99339**	**0.99421**	0.98790	0.99306
square root	**0.99312**	0.99326	0.99381	0.99294	**0.99839**

Table 3.3: Goodness of fit parameters R^2 obtained for different rate laws. Values of the best fit are shown in bold.

We examined the suggested rate laws by fitting to the dissolution profiles, excluding the initial and final parts of the profile which lie outside the fixed rate law regime. Goodness of fit parameters R^2 are given in Table 3.3. Results for a linear rate law are also included. From Table 3.3, we see that the square root law gives the best fit for the tablet, as expected. For the cubic crystal, the expected cube root law gives the best fit for the SPC/E and TIP3P

models, but not for SPC and TIP4P/2005, for which better fits are given by the square and linear laws, respectively. However, we note that in general all three rates laws give good fits to the dissolution profiles, and the differences in the R^2 values are too small to clearly identify the "best" rate law. One would need profiles on longer time scales (greater than the time needed for complete dissolution for the urea nanocrystals) to make clear distinctions. The rate constants obtained using the cube root law for cubic crystals and the square root law for the tablet are given in Table 3.4. These rate constants clearly show the model dependence noted above.

Cube			
Temperature (K)	300	320	340
SPC	0.57 ± 0.15	1.22 ± 0.12	2.71 ± 0.35
SPC/E	0.40 ± 0.08	0.88 ± 0.22	1.84 ± 0.36
TIP3P	0.65 ± 0.11	1.24 ± 0.20	2.63 ± 0.35
TIP4P/2005	0.58 ± 0.16	1.52 ± 0.21	2.64 ± 0.23
Tablet			
SPC	6.26 ± 0.03	n/a	n/a

Table 3.4: Rate constants (ns^{-1}) for urea dissolution in different water models at 300, 320, and 340 K. The rate constants for cubic and tablet-shaped crystals were obtained from fits to the cube root and square root laws, respectively.

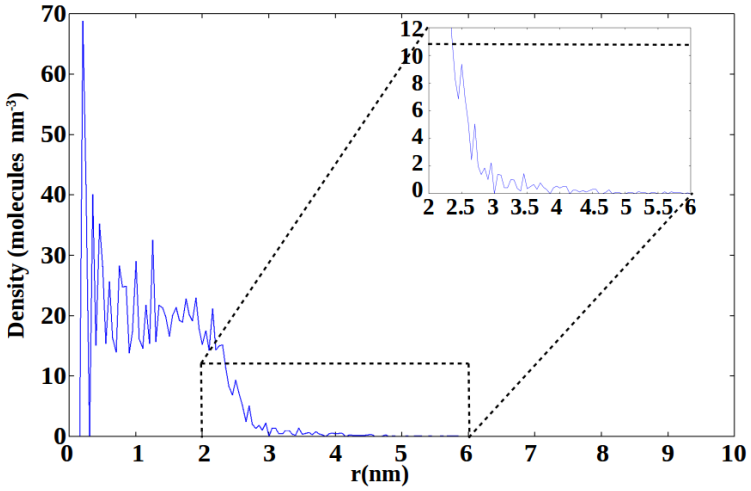

Figure 3.9: The radial density profile (molecules nm^{-3}) about the center of a cubic crystal in SPC water, measured at 0.75 ns. The dashed horizontal line in the inset indicates the saturation density.

The radial density profile of urea about the center of a dissolving cubic crystal is shown in Figure 3.9. We see that the urea density is nearly uniform in solution, and is much less than the saturation density. A density gradient occurs only very near the crystal surface, suggesting that the diffusion of urea into the bulk solution is not the rate determining step in the dissolution process. The rates we observe are qualitatively inconsistent with the observation of such a narrow diffusion layer.[6]

We also examined the thickness of the layer that would be required to explain the observed rate. We calculated $\Delta N/\Delta t$ for the cubic crystal in the fixed rate law stage at $\sim$ 0.75 ns, and estimated $dN/dt \simeq$ –130 molecules ns^{-1}. The diffusion coefficient for urea, $D \simeq 2.34 \times 10^{-9}$ m^2 s^{-1}, and the surface area of the solid at 0.75 ns is $\sim$ 63.62 nm^2. The saturation concentration C_s, is 10.82 molecules nm^{-3}. If there is a diffusion layer, the dissolution rate is given by, $dN/dt = -DSC_S/\delta$, implying that there has to be a diffusion layer of thickness $\sim$ 12.4 nm. This is obviously too thick to be relevant in our studies, as the crystal has a radius of $\sim$ 2.25 nm. Thus, we can safely conclude that detachment and not solute diffusion determines the dissolution rate.

3.4.2 Temperature dependence and activation energies

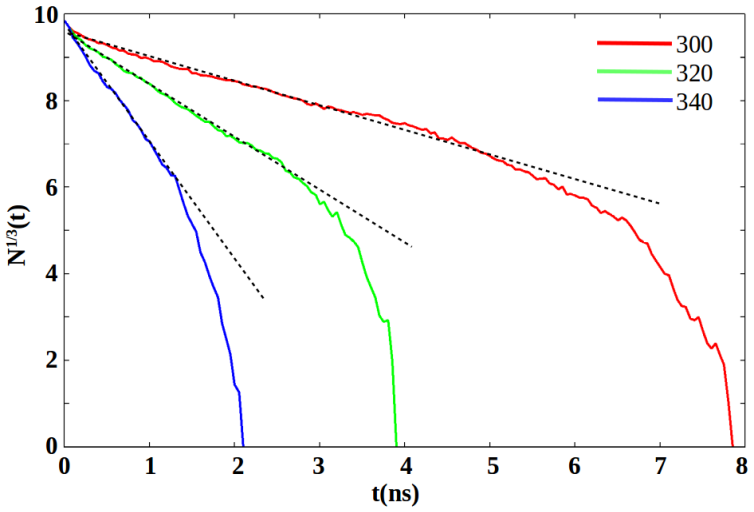

Figure 3.10: Fits to the cube root law for a cubic crystal in SPC water at 300, 320, and 340 K.

We would expect dissolution to be an activated process, and, in order to determine activation energies, simulations for the cubic crystal were carried out at three different temperatures, 300, 320, and 340 K. Rate constants (Table 3.4) were found by fitting the cube root law in the fixed rate law regime (excluding the initial and final region of the dissolution profiles). The cube root law gives an excellent representation of the dissolution profiles, as an example, the fits for the SPC model are shown in Figure 3.10. We also used rate constants obtained from the square root and the linear law to estimate the activation energy, and the energies are listed in Table 3.5.

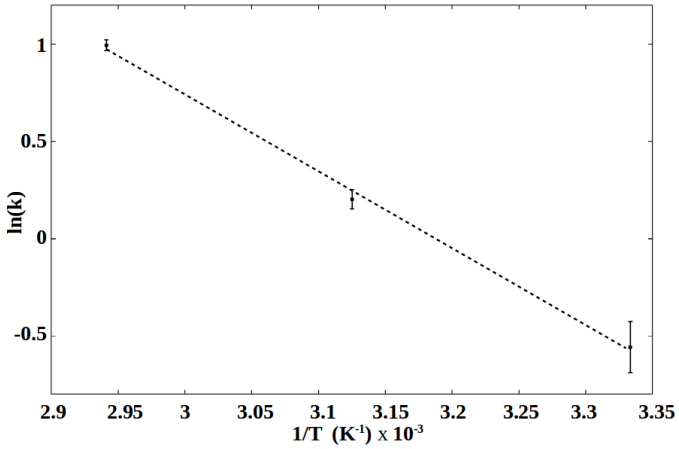

Figure 3.11: Fit to the Arrhenius equation of the rate constants obtained for a cubic crytal in SPC water at 300, 320, and 340 K.

For all water models considered, plots of of $\ln(k)$ vs. $1/T$ exhibit Arrhenius behavior ($ln(k) = ln(A) - E_a/RT$), as illustrated in Figure 3.11 for the SPC model. The activation energies of urea dissolution obtained for the different water models are listed in Table 3.5. The quoted standard deviations in the activation energies were obtained by dividing each profile into four equal parts and fitting to the rate law, such as to obtain four different estimates of the activation energy. We note from Table 3.5 that the activation energies associated with dissolution show no significant dependence on the water model employed, with the values for all models lying within overlapping standard deviations. For example, the activation energy obtained with the SPC/E model is nominally lower than that of SPC, yet the rate constant

obtained with SPC/E at 300 K is approximately only two-thirds that of SPC. The similarity of the dissolution activation energies suggests that some other effect is influencing the pre-exponential factor in the Arrhenius equation, and giving rise to the model dependence of the activation energies.

Water Model	Dissolution			Diffusion
	Cube root law	Square root law	linear law	
TIP4P/2005	32.21 ± 3.99	–	–	16.56 ± 0.30
TIP3P	29.51 ± 1.91	–	–	12.00 ± 0.37
SPC/E	32.24 ± 3.16	–	–	12.71 ± 0.43
SPC	32.88 ± 3.75	32.92 ± 2.01	33.03 ± 1.05	12.15 ± 0.28

Table 3.5: Activation energies (kJ mol^{-1}) for cubic crystal dissolution and urea diffusion.

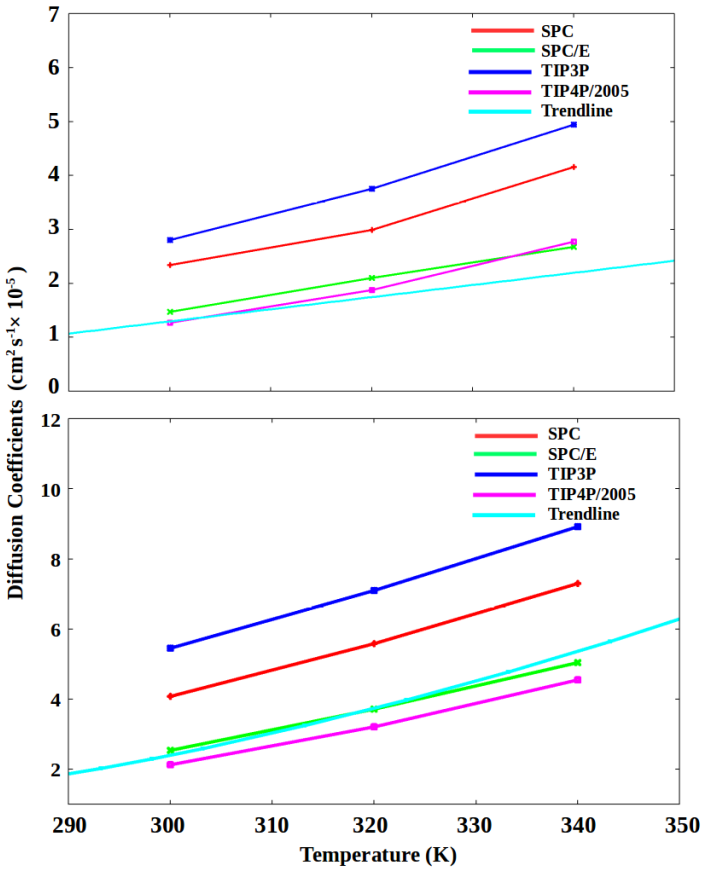

Figure 3.12: Diffusion coefficients of urea (top panel) and water (bottom panel) in solution. Experimental trendlines for urea[60] and water[61] are included.

One possibility we considered is that the diffusion rate of urea, or water (possibly both), is having some effect on the dissolution rate. To check this possibility, we calculated the diffusion coefficients of urea and water from mean square displacements at 300, 320, and 340 K, in equilibrium solutions after the entire crystal was dissolved. The activation energies for urea diffusion estimated from Arrhenius plots ($\ln(D) = \ln(A) - E_a/RT$) are included in Table 3.5, and we note that the activation energies for urea diffusion are much smaller than the corresponding values for dissolution. The diffusion coefficients for all four water models are plotted versus temperature in Figure 3.12, together with trendlines based on experimental data.[60,61] We notice that for urea the TIP4P/2005 results lie closest to the experimental trendline, whereas for water SPC/E agrees best with experiment, with TIP4P/2005 a close second.

From Figure 3.12, we see that for both urea and water the diffusion coefficients follow the order, TIP3P > SPC > SPC/E > TIP4P/2005), except at 340 K where the water diffusion coefficients for SPC/E and TIP4P/2005 are practically identical. We note that the order of urea diffusion coefficients for the three-point water models (TIP3P > SPC > SPC/E) matches the variation in the dissolution rates (Figure 3.2, and Table 3.4), which suggests that differing diffusion rates might be contributing to the different dissolution rates. However, the results for TIP4P/2005 do not fit this picture. The diffusion coefficients for TIP4P/2005 are similar to those of SPC/E, but for TIP4P/2005 the dissolution rate is considerably faster at all three temperatures. This suggests that some other, perhaps structural, effects are contributing to the different dissolution rates, but despite examining some possibilities such as radial distribution functions, urea-water hydrogen bonding, urea-water electrostatic interactions, and urea solvation energies, we could not identify any clear correlation that would explain all of the model-dependent variation in the dissolution rates.

3.5 Summary and conclusions

Employing MD simulations we have investigated in detail the dissolution of urea nanocrystals under sink conditions. Both cubic and tablet-shaped crystals were considered at temperatures of 300, 320, and 340 K. The GAFF forcefield,[23] which importantly gives a good representation of crystalline urea. was used together with four common water models. The qualitative dissolution mechanism was the same for all four water models considered, but there were surprisingly large differences in the dissolution rate.

We found that all urea crystals dissolved in three stages, similar to those observed for ionic NaCl nanocrystals.[6] Initially, loosely bound molecules located at corners and/or edges leave the crystal. After this process, the crystal takes on a solution annealed shape, which persists for most of the dissolution process during the stage we refer to as the fixed rate law regime. In the final stage, the dissolution profile departs from the governing rate law, crystalline structure is lost, and eventually the crystal completely vanishes into solution.

During the middle stage of dissolution, the rate is well described by a classical expression, which assumes that the rate is proportional to the active surface area of the crystal. Molecules are assumed to depart uniformly from the active surface area. After the initial stage, the active surface area of the initially cubic crystal is essentially spherical in shape, which leads to an integrated rate law of the cube root form. We show that the cube root law gives good fits to the simulation results for cubic crystals, over the intermediate stage of dissolution. We also show that the detachment of molecules from the crystal, and not the formation of a diffusion layer, is the rate determining step for the dissolution process. For cubic crystals, the rate constants obtained at different temperatures closely follow the Arrhenius equation, giving an activation energy of $\sim$ 32 kJ mol^{-1}. The activation energies obtained with all four water molecules are very similar, indicating that the differences in rate constant come through the pre-exponential factor in the Arrhenius equation. Our investigation of this issue suggested that some (but definitely not all) of the model dependence observed in the rate constants might be connected with the model dependence of the diffusion coefficients of water and/or

urea.

For the tablet-shaped nanocrystal, the overall dissolution mechanism was similar to that of cubic crystals, but in our simulations molecules only left the tablet from the curved surface, and never from the flat faces. Thus, we identified the active surface as cylindrical in shape, which gives a square root form for the integrated rate law. The square root law gave an excellent fit to the middle stage simulation results for the tablet-shaped crystal. However, we note that on the time scales of our simulations, there is not much difference between cube root and square root rate laws, and both give good fits to the simulation profiles.

Finally, we remark that the present simulations taken together with earlier work on the dissolution of NaCl crystals,[6] shows that at least for some crystals dissolution might be expected to follow a relatively uncomplicated three-stage mechanism. Importantly, the long middle stage of the dissolution process, during which the vast bulk of the crystal dissolves, is very well described by classical rate laws that depend only on the geometry of the active surface area, as determined after the crystal has solution annealed during the initial stage. This suggests that in some cases crystal dissolution studies may not require very long simulations. If the mechanism we have found for urea and NaCl applies, then it would be only necessary to simulate the initial stage of dissolution. This would allow one to identify the geometry of the active surface, and hence determine the rate law that governs the bulk of the dissolution process. More simulations of complex molecular solids are necessary in order to assess the generality of our observations, but the fact that similar mechanisms apply to crystals as different as NaCl and urea is an encouraging start.

Chapter 4

Dissolution of Aspirin Nanocrystals

4.1 Overview

The possibility of using classical dissolution models to predict dissolution rates of molecular solids is discussed in this chapter. Molecular dynamics simulation studies of dissolution of aspirin nanocrystals in water are reported. All the simulations were performed in a manner designed to prevent the build up of any significant concentration of aspirin in solution, and thus have a continuous dissolution of the aspirin nanocrystal. Cubic and cylindrical shaped crystals are studied to examine the effect of shape on dissolution. The effect of temperature is also examined. The dissolution is found to occur in four stages: an initial stage where the loosely bound molecules at the edges and corners go into the solution, after which the rounded cubic crystal transforms to a nearly cylindrically shaped crystal in a transformation stage. The transformation stage is absent in the dissolution of cylindrical crystals. After this stage the crystals dissolves at a nearly fixed rate, where the molecules leave the active surface (curved surface of cylindrical shape) nearly evenly, until the final dissolution stage, where the crystal dissolves rapidly because of its increasing instability due to its reduced size. The fixed rate stage of the dissolution, which is a major fraction of the whole dissolution run, is well described by classical rate equations which assume that the rate of dissolution is proportional to the active surface area of the crystal. The detachment of the molecules from the crystal is found to be the rate determining step for dissolution.

4.2 Introduction

In our continuing efforts to elucidate the dissolution process of molecular solids, we choose aspirin as the model molecule for further investigations. Aspirin is an Active Pharmaceutical Ingredient (API), which has been studied extensively since it's discovery. It along with most of the API's are known to have low solubility in water.[62] The dissolution of these solids influence important processes, such as drug delivery,[10] thus these are studies of high importance. However, due to poor solubility, simulation of the dissolution kinetics is very challenging.

There have been few studies which have investigated the dissolution of some APIs, but such studies only consider distinct faces in contact with the solvent. A study of acetaminophen dissolution in water by Gao and Olsen[16] revealed the significance of edges and corners in the initial stages of dissolution. So, a dissolution study of any solid would be incomplete without considering edges and corners. Elts et al.[17,63] investigated the dissolution of aspirin in water, and proposed an approach that was a combination of Molecular Dynamics (MD) and kinetic Monte Carlo (kMC) simulations. They used this approach to extend the time scales accessible to simulation, and found face displacement velocities of aspirin crystals.

Another recent study of the dissolution of the ionic crystal NaCl in water by Patey and Lanaro[6] used classical dissolution models[1,2,4,5] to interpret dissolution rates. They show that these models describe the dissolution profile of the crystal to a very good extent. We took the same approach in our study of urea in water described in Chapter 3, and found that we could predict the dissolution rate by considering only a fraction of the total dissolution run, by fitting the profiles to rate laws[3,46,47] obtained from classical models. However before coming to a general conclusion, we test the method for a molecular solid with very low solubility in water.

In this chapter we investigate the dissolution of aspirin nanocrystals in water to further support our conclusions based on the dissolution of urea nanocrystals. Aspirin was chosen because of it's relatively simple structure, contrasting low solubility with respect to urea in water, and the availability of a force field model, which replicates both solid and solution

phase properties. The complete dissolution of aspirin nanocrystal is studied and detailed descriptions of the various stages are presented. The effect of temperature and the initial shape of crystal on the dissolution rate is also investigated. The activation energy for the detachment process which is the rate determining step for aspirin dissolution is estimated.

The remainder of the chapter is organised as follows, models and methods used are given in section 4.3,detailed results are described and discussed in section 4.4, and conclusions is summarized in section 4.5.

4.3 Models and methods

We report various simulations of aspirin dissolution in water. In all simulations, the non-bonded interaction contains both the Lennard-Jones (LJ) and the electrostatic term as in Equation (3.1). The force-field parameters for aspirin were taken from the SwissParam[64] server, representing CHARMM-compatible parameters based on the Merlock Molecular Force Field (MMFF).[65] These parameters produced a stable crystal lattice, and the transition of the solid to the solution and vice versa could be describe qualitatively. The TIP3P[20] water model was used, as it gives the best agreement with experimental results for CHARMM model of aspirin crystals, and has been used in previous dissolution studies of CHARMM model of aspirin crystals.

We considered various shapes (Cubic and Cylindrical) of the Aspirin crystal to investigate the influence of shape on the dissolution rate, as used in earlier dissolution studies. The cubic crystal was generated by repeating the Aspirin unit cell in the directions of the three axes, and the cylindrical crystals were obtained by taking a cubic crystal and removing the molecules outside a circle centered about the symmetry axis of the cylindrical crystal.

Cubic crystals: These contained 800 molecules of aspirin and were generated by repeating the unit cell 5, 8 and 5 times along the different crystal axes. A cross section of the crystal along the (010) crystal plane, together with other crystal planes (100 and 001), are shown in Figure 4.1. A smaller cubic crystal containing 448 molecules was also used to test our method

for keeping the solution undersaturated.

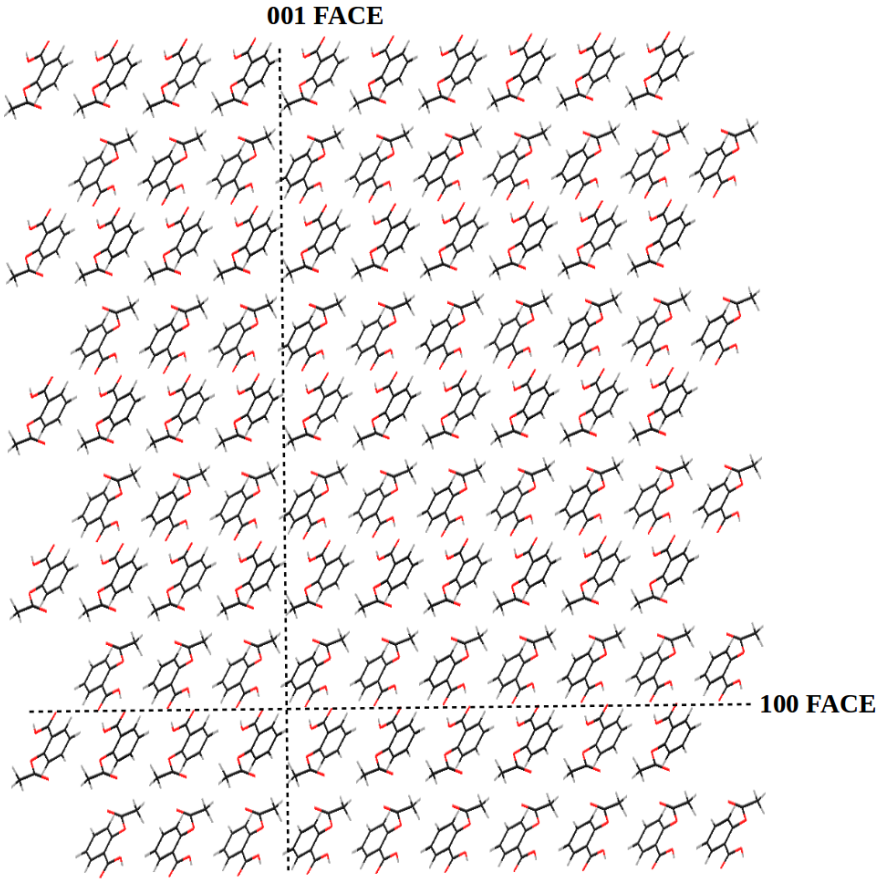

Figure 4.1: Schmatic representation of the cross section of a cubic crystal along the (010) crstal plane. The (100) and (001) planes lie perpendicular to the plane of the paper. The oxygen atoms are represented in red, hydrogen atoms in gray, and carbon atoms in black, respectively.

Cylindrical crystals: We investigated three different cylindrical crystals with different flat surfaces (the (100), (010) and (001) faces of the aspirin crystal). These contained 550, 464 and 490 molecules, respectively. Cylindrical crystals were generated by taking the cubic crystal and considering the three crystal axes as the axis for the three different cylindrical crystals, and then removing the molecules outside a circle of radius 2.4 nm centered about the symmetry axis of the cylindrical crystal. Top views (flat surface) and the side views (curved surface) of the three crystals are shown in Figure 4.2.

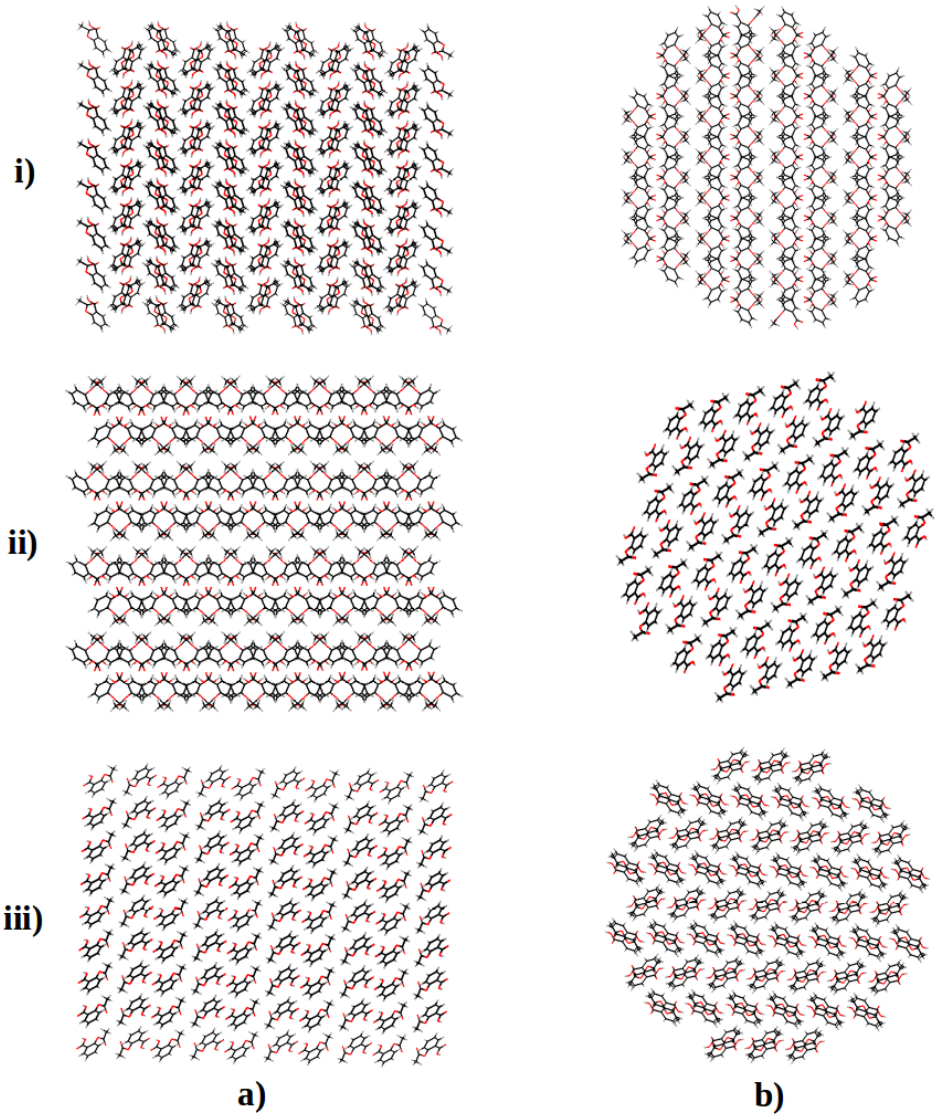

Figure 4.2: a) Side views (curved surface), and b) Top views (flat surface) of the cylindrical crystals. The crystals with (001), (010) and (100) faces as the flat surface are shown in i), ii) and iii), respectively. The oxygen atoms are represented in red, hydrogen atoms in gray, and carbon atoms in black, respectively.

All the simulations were carried out under NPT conditions with the pressure fixed at 1 bar. The details for the different initial configuration (temperature of the system and the number of aspirin and water molecules) in the various simulations are summarized in Table 4.1.

	Urea	Water	Temp(K)
Cube	800	39688	300
	800	39688	320
	800	39688	340
Cylinder	464	37970	300
	490	37445	300
	550	37442	300

Table 4.1: A summary of the number of aspirin and water molecules used, shapes of the initial crystals, and the temperatures at which simulations were performed

All simulations were performed using the GROMACS molecular dynamics package,[59] version package 4.5.5. The temperature was controlled using the Nosé-Hoover thermostat[35,36] with a time constant of 2.0 ps. The pressure was maintained by using the Parrinello-Rahman baraostat[37] with a compressibility of 4.46×10^{-5} bar^{-1} and a time constant of 2.0 ps. The time step for all the simulations was 1 fs. Periodic boundary conditions were used and the short range interactions were truncated at 1 nm. The electrostatic interactions were taken into account using the fourth order Particle-Mesh Ewald method[33] with a Fourier spacing of 0.12nm. All the bonds were constrained using the LINCS algorithm.[38]

The initial configurations for the simulations were generated by placing the crystal in the center of a cubic box of length 11 nm, and the box was filled with water molecules. The water molecules within the crystal lattice were then removed, and the system was relaxed for 0.2 ns keeping the aspirin molecules fixed, in order to equilibriate the solvent molecules around the crystal.

The experimental saturation concentration[66] of aspirin in water at 300-340 K correspond to aspirin mole fractions in the range 0.00112 - 0.0042. The extremely low solubility of aspirin results in the solution becoming oversaturated after just a small fraction of the crystal dissolved, and a new procedure was required to keep the solution undersatured. Earlier studies[17,63] used a slab of sticky dummy atoms to irreversibly trap molecules in solution (within a cutoff radius of the dummy atoms), by using a potential well. The trapped molecules were removed permanently from the system and constant undersaturation was observed throughout the dissolution. We devised another simple method to ensure undersaturation at all instances

during the simulation, resulting in continuous dissolution of the aspirin crystal.

Aspirin molecules which have passed into solution from the crystal and are outside a sphere (centered at the center of mass of the crystal) of fixed radius are removed at regular intervals. The box was then translated to make the center of the box coincide with the center of the aspirin crystal. This was done to ensure that the sphere always remained inside the box to prevent removal of any misrepresented aspirin molecules due to the periodic boundary conditions. The system was then allowed to evolve for another time interval, and the whole process for removal of aspirin molecules was repeated until complete dissolution of the crystal was achieved. The number of aspirin molecules leaving the crystal during different time intervals was monitored, and a time interval which ensured undersaturation at all instances during the simulation was chosen. The time interval used for removal of aspirin molecules was 2 ns for simulations at 300 K, and 1 ns for simulations at 320 and 340 K. The actual value of the radius did not greatly affect our results, as the dissolution profiles were qualitatively similar for values of 3.5 and 4.5 nm, as shown in Figure 4.3. The minor deviation at the end of the dissolution profile is mostly stochastic in nature, since very similar profiles were obtained when the radii were reversed at 240 ns (see inset in Figure 4.3). In our simulations we chose a value of 4.5 nm for the radius of the sphere beyond which aspirin molecules in solution were removed. The simulations required from 100 to 620 ns for complete dissolution, depending on the shape of the crystal and the temperature of the system.

The molecules were identified as a part of the crystal or the solution by means of a simple order parameter based on the number of neighbors. The number of neighbors was identified by counting the number of aspirin molecules within a sphere of radius 1.10 nm centered at the center of mass of the molecule. Molecules that were in the crystal had neighbors in the range 15-22, and the molecules in the solution had 1-3 neighbors. So, we chose the intermediate number 8 to be our cutoff value. A molecule with 7 or fewer neighbors was considered to be a part of the solution, and any molecule with 8 or more neighbors was identified as part of the crystal. The radius of the sphere for counting the neighbors and the cutoff value did not affect our results significantly, as the profiles were qualitatively similar for values of 0.70 and

1.40 nm.

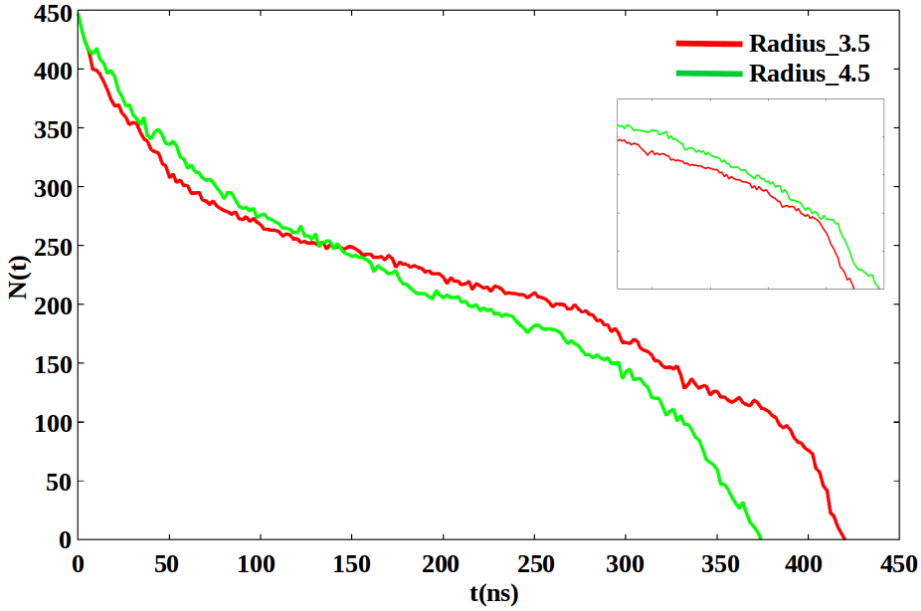

Figure 4.3: Dissolution profiles for the cubic crystal with different radii of the sphere used for removal of molecules in the solution. The profiles shown in the inset are for the same crystals with the sphere radii reversed at 240 ns in the dissolution runs.

4.4 Results and discussion

4.4.1 Stages of dissolution

The dissolution is found to occur in four different stages. The initial stage can be divided into two sub-stages, a very rapid dissolution of the loosely bound molecules, and a slower dissolution during which the crystal take a solution annealed shape. This is followed by a nearly steady dissolution rate for most of the dissolution run, after which the crystal dissolves at a very rapid rate as it becomes increasingly unstable due to its decreasing size.

A. Initial stage

During this phase of the dissolution, the loosely bound molecules at the corners and edges of the crystal get detached and passes into solution. This process depends on the shape of

the crystal, as the shape determines the number of molecules on the edges and corners of the crystal, and leads to exposure of more crystal molecules to the solution, thus enabling the solution to anneal the crystal to a shape that gives an active surface from which the molecules leave at a nearly even rate.

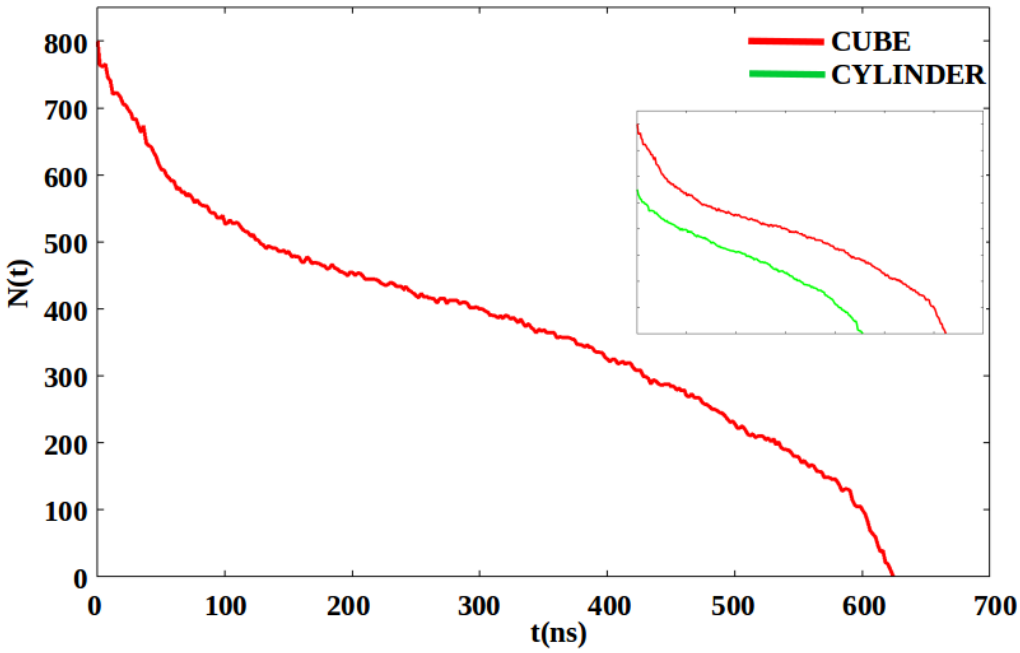

Figure 4.4: The dissolution profile for a cubic crystal displayed as the number of molecules vs time. The profiles for a cubic crystal and a cylindrical crystal with the (100) face as its flat surface are shown in the inset.

A dissolution profile for an initially cubic crystal is plotted in Figure 4.4, and snapshots of the crystal at various points in the dissolution run are shown in Figure 4.5. For the cubic crystal, as can be seen from the dissolution profile in Figure 4.4, the crystal loses nearly 100 molecules in the first 20 ns of the dissolution run. It is also evident from the snapshots in Figure 4.5 that during the first 20 ns the crystal has lost nearly all of the molecules at the edges and corners. After these initial detachments, the crystal still has a basically cubic shape with six faces and rounded edges and corners. It takes the cubic crystal another 100 ns to take a cylindrical shape, which is the next phase of the dissolution, and is detailed in the next section.

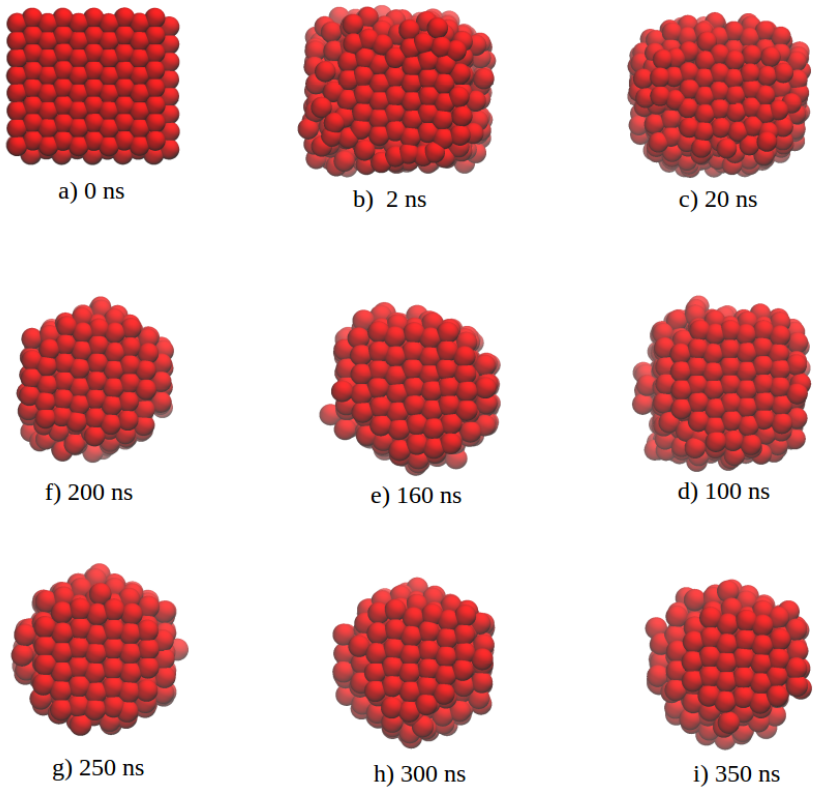

Figure 4.5: Snapshots of the (100) face corresponding to different points in the dissolution profile of a cubic crystal. Each red sphere indicates an aspirin molecule.

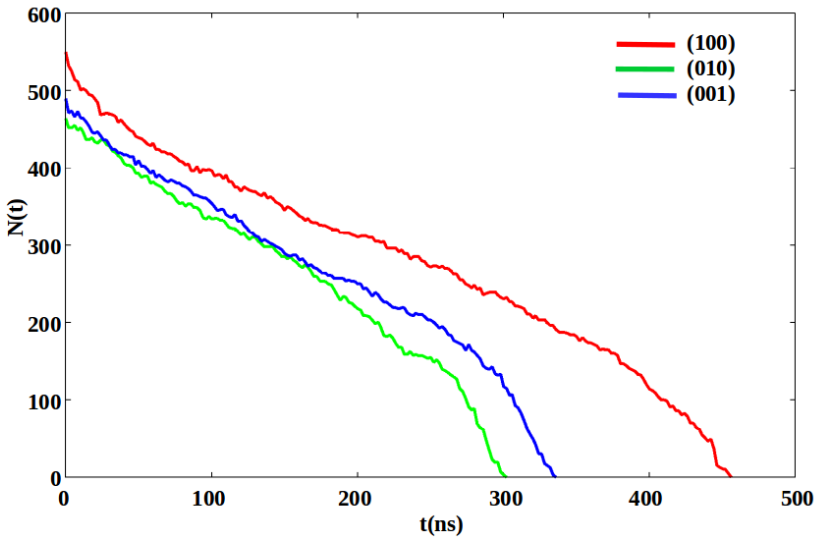

Figure 4.6: Dissolution profiles for three cylindrical crystals with different flat surfaces.

For the three different cylindrical crystals, there is a similar trend in the dissolution profile, where they lose the molecules on the edges of the crystal very rapidly in the first part of the dissolution run. This is evident from the dissolution profiles in Figure 4.6. Also it can be seen from the snapshots of the cylindrical crystal in Figure 4.7, that the crystal loses molecules from the curved surface and not the flat face. This stage is followed by a nearly fixed rate dissolution, where molecules come off the crystal evenly from the active surface area.

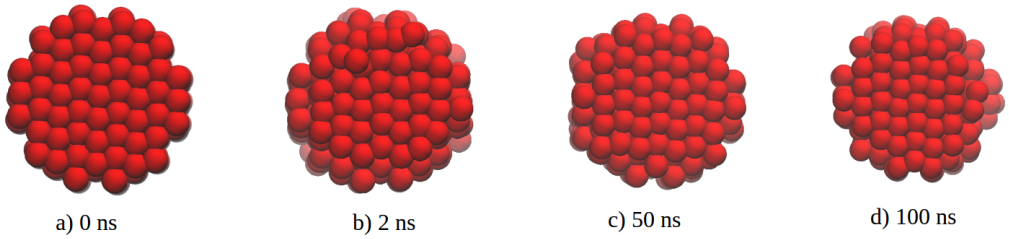

Figure 4.7: Snapshots corresponding to different points in the dissolution profile of a cylindrical crystal with the (100) face as its flat surface. Each red sphere indicates an aspirin molecule.

B. Transformation stage

The rounded cubic crystal after the initial rapid dissolution stage still has the three crystal faces (100, 001, and 010) that were present in the initial crystal. These surfaces have different displacement velocities,[17] with the (100) face having the smallest, and the other faces (010) and (001) having similar velocities. This makes the (100) face the most stable surface of all the surfaces exposed to solution. The water gradually consumes molecules from corners of the other surfaces at a very rapid rate, in comparison with molecules from the (100) face. This results in the formation of a nearly cylindrical shaped crystal with the (100) face as the flat surface, and the other faces being less stable, are attacked to form a nearly uniform curved surface. This transformation of the rounded cubic crystal to a nearly cylindrical crystal takes around 100 ns, and can be seen from the snapshots of the dissolution run shown in Figure 4.5. Once the cylindrical crystal is formed in solution, molecules start to come off the curved surface evenly resulting in a nearly fixed rate of dissolution, and this cylindrical shape of the

crystal is retained for most of the dissolution run, as evident from Figure 4.5.

The active surface for cylindrical crystals are the curved surfaces from the beginning of the dissolution run, which is the solution annealed stable shape for these crystals. This is the reason we do not see a transformation stage in the cylindrical crystals, and they directly transition to the fixed rate law stage after the initial stage.

C. Fixed rate law stage

After the initial stages of dissolution, all the crystals follow a similar trend. The dissolution profile remains almost linear during this stage, which is a major part of the whole dissolution run. The crystal retains the stable shape (cylindrical), attained after the initial stages of the dissolution run, throughout this stage.

During this phase of dissolution, molecules leave the crystal evenly from the active surface area formed after the initial stages. The curved surface of the cylindrical crystals is identified as the active surface in these crystal, as no molecules leave the crystal from the flat surfaces. This essentially uniform detachment of molecules from the active surface results in a dissolution process which follows a fixed rate law, until the final rapid dissolution stage.

Next we evaluate the effect of crystal shapes on the dissolution rate and also compare the dissolution profile in the fixed rate law stage with different classical models mentioned above.

D. Influence of crystal shape

Cubic and cylindrically shaped crystals were used to investigate the effects of shape. It is evident from the dissolution profiles (Figures 4.4 and 4.6) that all the crystals have similar initial and final stages, where there is a rapid dissolution of the molecules from the crystal (details in sections 4.4.1.A and 4.4.1.F, above). Cylindrical crystal do not undergo the transformation stage, where cubic crystals transform from a rounded cubic structure to a nearly cylindrical structure (see section 4.4.1.B for details).

Once this transformation is complete, all crystals have a nearly fixed rate of dissolution. It can be seen from the inset in Figure 4.4 that the dissolution profile for the fixed rate stage

of a cylindrical crystal with the (100) face as the flat surface is qualitatively similar to that of a cubic crystal. An interesting observation from these profiles is that the rate of dissolution of a crystal with more than one flat surface (having different displacement velocities) is very similar to a cylindrical crystal with the most stable face of the crystal as the flat surfaces.

E. Comparison with dissolution models

As discussed before, there have been a number of dissolution studies over the last century, and several models in the form of differential and integral rate laws have been proposed. We employ a very simple rate law to describe the fixed rate stage of these dissolution profiles. Since all of our simulations have been carried out under sink conditions, the detachment process is expected to be the rate determining step, and the rate can be described as

$$\frac{dN(t)}{dt} = -kS_{active}(t), \tag{4.1}$$

where $N(t)$ is the number of molecules in the crystal at time t, $S_{active}(t)$ is the active surface area where the detachment process takes place, and k is a constant. This law, which takes into account the changing surface area, was first suggested by Brunner and Tolloczko.[2]

The differential form is used to get the integral rate law using different forms of the active surface area, $S_{active}(t)$. The active surface area in our case is the curved surface of the cylindrical structure. Thus, using area to volume relationships gives us the relation $S_{active}(t) \propto N^{1/2}(t)$, which leads to the integrated rate law

$$\sqrt{N(t)} = \sqrt{N_0} - kt, \tag{4.2}$$

where k is the rate constant. The fixed rate regimes for the crystals were then compared with the law, by fitting the integrated rate law equation to the dissolution profiles. The goodness of fit parameters, R^2, for each crystal are listed in Table 4.2. Results for the cube root and the linear rate laws are also included in the table. The best fits clearly corresponds to the rate law derived above for the cylindrical crystals, while in case of the cubic crystal the differences

in the goodness of fit parameters are too small for us to draw any firm conclusion.

	Cubic	Cylindrical		
		(100) face	(010) face	(001) face
linear	**0.9892**	0.9922	0.9940	0.9937
square root	0.9852	**0.9950**	**0.9941**	**0.9976**
cube root	0.9829	0.9947	0.9930	0.9976

Table 4.2: Goodness of fit parameters R^2 obtained for different rate laws

We also argue that the diffusion of the molecules in the solution is not the rate determining step, as the simulation was done in a way to prevent build up of any diffusion layer around the crystal. We have calculated the diffusion coefficients of aspirin in the solution at 300, 320, and 340 K, and the values are listed in Table 4.3. The activation energy for aspirin diffusion was estimated from the Arrhenius equation ($ln(D) = ln(A) - E_a/RT$), and is 27.82 ± 4.24 kJ mol^{-1}. It can be noted that the value is significantly smaller than the activation energy for dissolution (48.31 ± 6.63 kJ mol^{-1}, see section 4.4.2, below). Thus, the diffusion layer model does not apply to the dissolution of the Aspirin.

	Diffusion Coeffecients ($cm^2\ s^{-1} \times 10^{-5}$)	
	TIP3P	TIP4P/2005
300 K	0.88 ± 0.53	0.78 ± 0.25
320 K	1.90 ± 0.50	1.43 ± 0.43
340 K	3.24 ± 0.67	1.97 ± 0.85

Table 4.3: Diffusion coefficients of aspirin in solution.

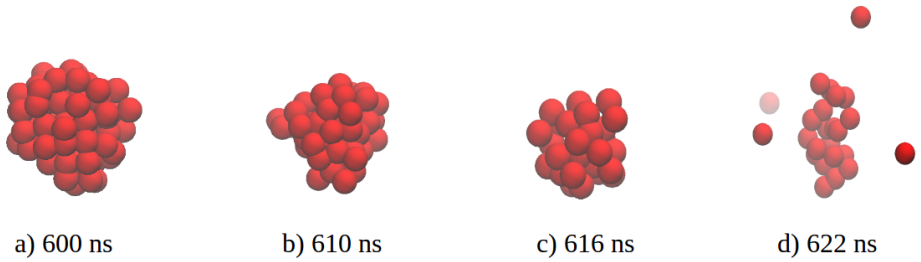

Figure 4.8: Snapshots of the last stages in the dissolution profile of a cubic crystal. Each red sphere indicates an aspirin molecule.

F. Final stage

Dissolution profiles in Figure 4.4, suggest that there is a sharp increase in the dissolution rate during the final stages of the dissolution run. The crystal becomes very unstable, and disappears rapidly once it has been reduced to a very small size. During this phase the crystal starts to loose its crystalline structure and then disintegrates completely. The is evident in the snapshots shown in Figure 4.8.

4.4.2 Temperature dependence and activation energy

The detachment of the molecules from the crystal is expected to be an activated process, and to estimate the activation energy we carried out simulations of the cubic crystal at three different temperatures, 300, 320, and 340 K. The rate constants were calculated by fitting the fixed rate stage of the dissolution profiles to the square root law. The profiles fit the rate law excellently, as shown in Figure 4.9. The rates follow the Arrhenius equation (Figure 4.10)

$$ln(k) = ln(A) - E_a/RT \ , \tag{4.3}$$

giving an activation enrgy of 48.31 $\pm$ 6.63 kJ mol^{-1}.

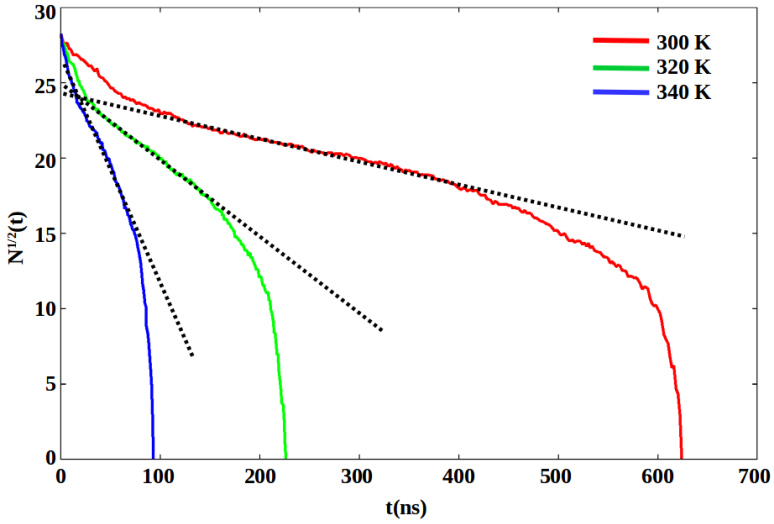

Figure 4.9: Fits to the square root law for a cubic crystal at temperatures of 300, 320, and 340 K.

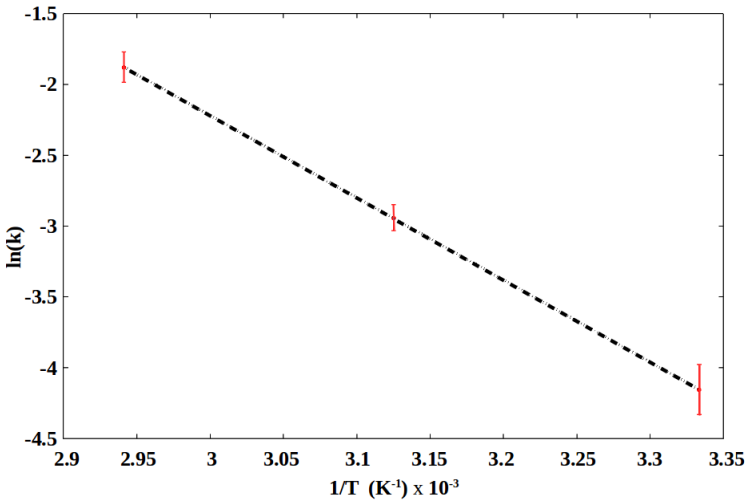

Figure 4.10: Fits to the Arrhenius equation of the rate constants obtained for a cubic crystal at temperatures of 300, 320, and 340 K.

The standard deviations shown as error bars in Figure 4.10 were calculated by dividing the fixed rate stages of the dissolution profiles into five equal parts, and rate constants were calculated by fitting each part to the square root law. These five different rate constant were then used to calculate the standard deviation, shown as error bars in Figure 4.10. Similarly, the five different sets of rate constants were then used to calculate the standard deviation in activation energy.

4.4.3 Model dependence

The dissolution of aspirin nanocrystals in water was also studied using the TIP4P/2005[21] water model. The qualitative dissolution profile for the cubic crystal does not depend on the water model used, and we see the four stage dissolution in both cases. However, the dissolution rate is found to depend on the water model used, with the dissolution in the TIP4P/2005 water model occuring considerably slower than in TIP3P water. The activation energy for dissolution in TIP4P/2005 water model was estimated using the Arrhenius behavior of the rate constants at 320 and 340 K, and was found to be 52.72 kJ mol^{-1}. The plot of the dissolution profile in TIP4P/2005 water model is shown in Figure 4.11, and it can be noted

that the profiles are well fit by the square root law.

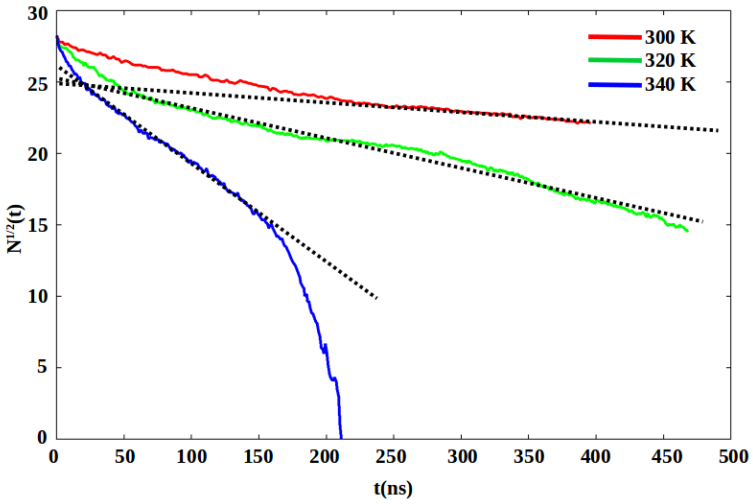

Figure 4.11: Fits to the square root law for a cubic crystal in TIP4P/2005 water at temperatures of 300, 320, and 340 K.

The dependence of the dissolution rate on the water model used can be explained by the slight difference in activation energy for the water models, despite the high standard deviation in the estimation of the activation energy. We assume that the activation energy is dependent on both the crystal and crystal-water interface, though a very weak dependence on the latter. This is justified as we found that the aspirin molecules interact with TIP4P/2005 water model more strongly, thus they may form a more stable crystal-water interface in TIP4P/2005 water model, leading to a slightly bigger activation barrier, and a slower dissolution rate. Other factors such as solvation time, aspirin-water hydrogen bonding, and diffusion coefficients (see Table 4.3), are very similar for both the cases.

4.5 Summary and conclusions

Molecular dynamics simulations were carried out to study the dissolution of a molecular model for aspirin nanocrystals of different shapes and size in detail. Cubic and cylindrically shaped crystals were used in simulations, where all dissolution was performed under sink conditions. In our studies, the dissolution was found to occur in four stages for cubic crystals and three

stages for cylindrical crystals. The initial stage, where loosely bound molecules at the corners and edges of the crystal pass into the solution, was common in all the simulations. This stage depends on the initial structure of the crystal as the structure influences the number of molecules on the edges/corners of the crystal. After the initial stage, both crystals retained their initial shape with the edges being smoothed by the solution. A transformation stage, which occurred only in the dissolution of cubic crystals, transformed the well rounded cubic crystal into a nearly cylindrical shape. Once both crystals had acquired a nearly cylindrical shape, molecules left the crystal from the curved surface of the cylindrical crystal essentially evenly, giving a nearly fixed dissolution rate until the final stage of dissolution, where the crystal dissolves at a very rapid rate because of its increasing instability due to the reduction in size. The stages appears to be similar to that of the ionic NaCl nanocrystals and molecular urea nanocrystals.

The fixed rate stage of the dissolution was well described by considering the rate to be proportional to the active surface area of the crystal. For both the crystals, the active surface area was the curved surface of the cylindrical shape they attain after the initial stage. Thus we obtain the square root law, which is appropriate for crystals having cylindrical shape. We show that the square root law describes the fixed rate stage very well, by examining the goodness of the fit parameter for each simulation. We also show that the detachment of molecules from the crystal is the rate determining step, and not the formation of a diffusion layer around the crystal. We determined the activation energy for the detachment process by fitting the rates of dissolution of the cubic crystal at three different temperatures 300, 320 and 340 k to the Arrhenius equation. The activation energy was approximately 48.31 kJ mol^{-1}, which is significantly bigger than the value obtained for urea dissolution ($\sim$ 32 kJ mol^{-1}).

We conclude from our simulations of urea and aspirin nanocrystals, that the classical models give an accurate description of the fixed rate stage of dissolution of these nanocrystal. Thus we can use these models to study the dissolution of different molecular nanocrystals, and predict the rates by running only a fraction of the simulation, therefore reducing the problem of the long time scales required for a dissolution run.

Chapter 5

Summary and Conclusions

5.1 Summary

Dissolution research has been developing for over a century as a field in physical chemistry, and different models have been put forward as a description of the dissolution process. However, in the last few decades dissolution of microscopic molecular crystals has gained considerable interest, because of the importance of dissolution properties in drug bioavailability. However, most of the active pharmaceutical ingredients exhibit poor solubility or permeability, and thus simulations of the dissolution process is very challenging, even after the immense increase in computational power. In this thesis, we investigated the dissolution process of molecular solids, using urea and aspirin nanocrystals as models, and propose a method to predict dissolution rates by analyzing the results of the simulations.

In Chapter 2, the models used to represent urea, aspirin and water molecules in the simulation are presented, as well as the different algorithms and methods of the molecular dynamics simulations.

Chapter 3 describes an investigation of the dissolution process of urea nanocrystals in water. We found that the dissolution of urea can be described as a three step process, where the crystal first looses the edges and corners very rapidly, followed by a steady dissolution rate until it reaches a certain size ($\lesssim$ 200 molecules), and then losses its crystalline structure and dissolves completely into solution. It was also found that the rate laws obtained from the classical models described the fixed rate regime of the dissolution profile to a very good extent. Additionally, dissolution was found to be an activated process, with detachment of molecules from the crystal being the rate determining step. The activation energy for urea

dissolution was found to be $\sim$ 32 kJ mol^{-1} and was similar for different water models used. However, the dissolution rate varied across the water models, implying some dependence on the pre-exponential factor in the Arrhenius equation.

In Chapter 4 we further investigated the dissolution process by using aspirin nanocrystals as a model. The dissolution was found to occur in four steps, with an additional transformation stage where the crystal, with molecules at the edges and corners gone into the solution, dissolves slowly to take a solution annealed shape before the steady dissolution regime. The rate law obtained from the classical model was found to describe the steady part of the dissolution profile again to a very good approximation. The activation energy was found to be $\sim$ 49 kJ mol^{-1}, which is perhaps expected given the low solubility of aspirin as compared with urea in water.

Based on our simulation results, it can be concluded that classical rate laws can be used to predict dissolution rates for some molecular solids, by fitting an early part of the dissolution profile to simple rate law expressions.

5.2 Future directions

Our results show a surprisingly strong dependence of the dissolution rate on the water model used for simulation. This implies that small differences in the electrostatic charges on the water model influences the dissolution rate, and since the majority of the dissolution processes of interest involve complex mixtures of different solvents (water, acids, and bases), it would be of interest to examine if the proposed dissolution mechanism is valid in these more complex situations.

A partial explanation for the difference in dissolution rates came from the difference in diffusion coefficients. We found that the diffusion coefficients of urea, and water models are directly proportional to urea dissolution rates in three-point water models. However, this did not explain the dissolution rates in the four-point water model. Another explanation was the difference in activation energies, which could lead to different rates, but the large standard

deviations in the activation energies makes it difficult to evaluate this possible explanation. Thus, more studies are definitely required to study this difference in dissolution rate across models.

Bibliography

[1] A. A. Noyes and W. R. Whitney, J. Am. Chem. Soc. **19**, 930 (1897).

[2] L. Bruner and S. Tolloczko, Z. Phys. Chem. 283 (1900).

[3] A. Hixson and J. Crowell, Ind. Eng. Chem. **23**, 1160 (1931).

[4] E. Brunner, Z. phys. Chem. **43**, 56 (1904).

[5] W. Nernst, Z. phys. Chem. **47**, 52 (1904).

[6] G. Lanaro and G. N. Patey, J. Phys. Chem. B **119**, 4275 (2015).

[7] M. Wilderman, Z. Phys. Chem. **66**, 445 (1909).

[8] A. B. Zdanovskii, Zhur. Fiz. Khim. **20**, 869(1946).

[9] P. V. Danckwerts, Ind. Eng. Chem. **43**, 1460 (1951).

[10] A. Dokoumetzidis, and P. Macheras, Int. J. Pharma. **321**, 1 (2006).

[11] S. S. Jambhekar and P. J. Breen, Drug Discovery Today **18**, 1173 (2013).

[12] J. B. Dressman, G. L. Amidon, C. Reppas and V. P. Shah, Pharm. Res. **15**, 11 (1998).

[13] O. Anand, X. Y. Lawrence, D. P. Conner and B. M. Davit, AAPS J. **13**, 328 (2011).

[14] J. Siepmann and F. Siepmann, Int. J. Pharma. **453**, 12 (2013).

[15] S. Piana and J. D.Gale, J. Am. Chem. Soc. **127**, 1975 (2005).

[16] Y. Gao and K. W. Olsen, Mol. Pharmaceutics **10**, 905 (2013).

[17] E. Elts, M. Greiner and H. Briesen, Crys. Growth Des. **7**, 4154 (2016).

[18] H. J. Berendsen, J. P. Postma, W. F. van Gunsteren and J. Hermans, Intermolecular forces, Springer:Dordrecht, Netherlands, 331 (1981).

[19] H. J. Berendsen, J. R. Grigera and T. P. Straatsma, J. Phys. Chem. **91**, 6269 (1987).

[20] W. L. Jorgensen, J. Chandrasekhar, J. D. Madura, R. W. Impey and M. L. Klein, J. Chem. Phys. **79**, 926 (1983).

[21] J. L. Abascal and C. Vega, J. Chem. Phys. **123**, 234505 (2005).

[22] P. Xiu, Z. Yang, B. Zhou, P. Das, H. Fang and R. Zhou, J. Phys. Chem. B **115**, 2988 (2011).

[23] G. A. Özpınar, W. Peukert and T. Clark, J. Mol. Model. **16**, 1427 (2010).

[24] G. A. Özpınar, F. R. Beierlein, W. Peukert, D. Zahn and T. Clark, J. Mol. Model. **18**, 3455 (2012).

[25] P. Vaughan and J. Donohue, Acta. Crystallogr. **5**, 530 (1952).

[26] J. E. Worsham, H. A. Levy and S. E. Peterson, Acta. Crystallogr. **10**, 319 (1957).

[27] S. Swaminathan and B. M. Craven, Acta. Crystallogr. Sect. B **40** , 300 (1984).

[28] C. C. Wilson, New J. Chem. **26**, 1733 (2002).

[29] M. Greiner, E. Elts, J. Schneider, K. Reuter and H. Briesen, J. Cryst. Growth **405**, 122 (2014).

[30] R. W. Hockney, S. P. Goel and J. Eastwood, J. Comp. Phys. **14**, 148 (1974).

[31] M. P. Allen and D. J. Tildesley, *Computer simulation of liquids*, Oxford University Press:New York, **1989**.

[32] P. P. Ewald, Ann. Phys. **369**, 253 (1921).

[33] T. Darden, D. York and L. Pedersen, J. Chem. Phys. **98**, 10089 (1993).

[34] J. W. Cooley and J. W. Tukey, Math. Comp. **19**, 297 (1965).

[35] S. Nosé, J. Chem. Phys. **81**, 511 (1984).

[36] W. G. Hoover, Phys. Rev. A **31**, 1695 (1985).

[37] M. Parrinello and A. Rahman, J. Appl. Phys. **52**, 7182 (1981).

[38] B. Hess, H. Bekker, H. J. Berendsen and J. G. Fraaije, J. Comput. Chem. **18**, 1463 (1997).

[39] P. H. Stahl and C. G. Wermuth, *Handbook of Pharmaceutical Salts: Properties, Selection and Use*, Verlag Helvetica Chimica Acta, Zürich, 2002.

[40] J. D. Wuest, Nat. Chem. **4**, 74 (2012).

[41] H. Crawford and J. McIntosh, Arch. Int. Med. **36**, 530 (1925).

[42] J. H. Meessen and H. Petersen, *Ullmann's Encyclopedia of Industrial Chemistry.* Wiley Online Library, (1996).

[43] M. Dunky, Int. J. Adhes. Adhes. **18**, 95 (1998).

[44] W. Raab, Cosmet. Toiletries **105**, 97 (1990).

[45] P. Costa and J. M. S. Lobo, Eur. J. Pharm. Sci. **13**, 123 (2001).

[46] P. Niebergall, G. Milosovich and J. Goyan, J. Pharm. Sci. **52**, 236 (1963).

[47] W. Higuchi and E. Hiestand, J. Pharm. Sci. **52**, 67 (1963).

[48] F.-M. Lee and L. E. Lahti, J. Chem. Eng. Data **17**, 304 (1972).

[49] R. A. Kuharski and P. J. Rossky, J. Am. Chem. Soc. **106**, 5786 (1984).

[50] M. Salvalaglio, T. Vetter, F. Giberti, M. Mazzotti and M. Parrinello, J. Am. Chem. Soc. **134**, 17221 (2012).

[51] J. F. Brandts and L. Hunt, J. Am. Chem. Soc. **89**, 4826 (1967).

[52] D. B. Watlaufer, S. K. Malik, L. Stoller and R. L. Coffin, J. Am. Chem. Soc. **86**, 508 (1964).

[53] M J. Schick, J. Phys. Chem. **68**, 3585 (1964).

[54] E. M. Duffy, D. L. Severance and W. L. Jorgensen, Isr. J. Chem. **33**, 323 (1993).

[55] L. J. Smith,H. J. Berendsen and W. F. van Gunsteren, J. Phys. Chem. B **108**, 1065 (2004).

[56] W. L. Jorgensen and J. D. Madura, Mol. Phys. **56**, 1381 (1985).

[57] C. Vega and J. L. Abascal, Phys. Chem. Chem. Phys. **13**, 19663 (2011).

[58] C. M. Riley and T. W. Rosanske, *Development and Validation of Analytical Methods.*; Elsevier Science: New York, (1996).

[59] S. Pronk, S. Páll, R. Schulz, P. Larsson, P. Bjelkmar, R. Apostolov, M. R. Shirts, J. C. Smith, P. M. Kasson and D. van der Spoel, Bioinformatics **29**, 845 (2013).

[60] A. Sadeghi, D. Kissel and M. Cabrera, Soil Sci. Soc. Am. J. **52**, 46 (1988).

[61] M. Holz, S. R. Heil and A. Sacco, Phys. Chem. Chem. Phys. **2**, 4740 (2000).

[62] N. Variankaval, A. S. Cote and M. F. Doherty, AIChE J. **54**, 1682 (2008).

[63] M. Greiner, E. Elts and H. Briesen, Mol. Pharm. **11**, 3009 (2014).

[64] V. Zoete, M. A. Cuendet, A. Grosdidier, and O. Michielin, J. Comput. Chem. **32**, 2359(2011).

[65] T. A. Halgren, J. Comput. Chem. **17**, 490(1996).

[66] A. Apelblat and E. Manzurola, J. Chem. Thermodyn. **31**, 85(1999).